Theses and Dissertations

2016

# Factors Influencing The Collagen Fiber Angle Distribution in The Mouse Aorta

Shana Roach Watson
*University of South Carolina*

Follow this and additional works at: http://scholarcommons.sc.edu/etd

Part of the Other Medical Sciences Commons

www.manaraa.com

FACTORS INFLUENCING THE COLLAGEN FIBER ANGLE DISTRIBUTION IN THE MOUSE AORTA

by

Shana Roach Watson

Bachelor of Science
Clemson University, 2011

Submitted in Partial Fulfillment of the Requirements

For the Degree of Doctor of Philosophy in

Biomedical Science

School of Medicine

University of South Carolina

2016

Accepted by:

Susan Lessner, Major Professor

John Eberth, Chairman Examining Committee

Norma Frizzell, Committee Member

Chandrashekhar Patel, Committee Member

Michael Sutton, Committee Member

Lacy Ford, Senior Vice Provost and Dean of Graduate Studies

DEDICATION

Mom, you have always been a major supporter of education.  I give you all the credit for my accomplishments. I can assure you, greater is coming.

To my only and older sibling, Terrell: Your fulfillment as a father figure has been a treasure and I have never told you but, "Thank you".

To the Roach family, you guys are the best support system <u>anyone</u> could ever even wish for. I have carried your prayers along the way.

*The Bible says, "To write a vision and make it plain."*

*-Habakkuk 2:2*

Randall, thanks for teaching me to be imaginative and to believe in myself. Without your encouragement and partnership, I do not think I would have had a vision to write.

# ACKNOWLEDGEMENTS

I would like to thank my advisor, Dr. Susan Lessner, for her guidance throughout my graduate career. She has shown me that women can be leaders in STEM fields. In addition I would like to acknowledge the current and former members of the Lessner lab, John Johnson, Henry Bateman, Ying Wang, Nishant Karasala, Mohamed Gabr, and Lindsey Davis.  Each one of you has taught me something different and I am appreciative. My undergraduate assistants, Marcella Marks and Savannah Han, were a major help.

Thanks to my collaborators, Dr. Edsel Pena and Piaomu Liu for providing statistical analysis of multiple projects.  Further, I would like to thank the members of my committee, Drs. John Eberth, Norma Frizzell, Chandrashekhar Patel, and Michael Sutton for their encouragement and professional advice. Sincerest thanks to Merissa Baxter and my PREP mentors Drs. Bert Ely and Richard Hunt for pushing me towards success from the very start.

*And in memory of my ASBMB mentor, Dr. Marion B. Sewer who had a passion for increasing diversity and inclusion in science.*

# ABSTRACT

The aortic extracellular matrix (ECM) consists of microstructural proteins, collagen and elastin, together with proteoglycans and other components. The matrix metalloproteinases (MMPs) are proteolytic enzymes that influence morphological and structural changes in the ECM and can degrade the matrix as it responds to cellular behaviors such as angiogenesis, apoptosis, proliferation, and migration. Collagen is the most important component among the extracellular proteins because it provides strength and stability to the tissue. Changes in collagen content play a major role in the development of atherosclerosis. These changes can be induced by increased or decreased proteinase activity. Therefore, we studied the collagen fiber angle distribution in mouse models of atherosclerosis with or without a deficiency of a selected MMP. Quantification of the collagen fiber data is meaningful in providing insight into the mechanical behavior of the artery and leads to an understanding of how the diseased aorta maintains homeostasis. Furthermore, such data can be utilized to increase the understanding of disease progression, including but not limited to atherosclerosis and aortic aneurysm development.

We characterized collagen fiber angles in mouse models of atherosclerosis which were fed a control chow diet or a high-fat Western diet for 6 months. To visualize collagen, we imaged the mouse thoracic and abdominal

aorta using second-harmonic generation (SHG) microscopy. Angle measurements were acquired using a well-established computer software program, *Continuity 6.4b*. The angle measurements were exported into bivariate histograms. We then designed a multiple regression analysis to compare the distributions of absolute angles between two diet groups, controlling for diet, mouse strain, anatomical location, and radial position in the aortic wall. Data extracted from bivariate histograms were analyzed in R, a programming language and statistical software.

In trying to understand the changes seen between chow diet and Western diet fed mice, we began to study physiological variables such as blood pressure and blood flow velocity. While we did not find any differences in the hemodynamics, we were able to determine that factors beyond atherogenesis, for example aging, influenced aortic collagen fiber angle distributions. With aging and atherosclerosis, the extracellular matrix may experience an increase in collagen content and fibrous tissue. We evaluated changes in fractional collagen amount, in particular, collagen type I. To understand if changes in collagen fibers are initiated by endothelial dysfunction (a pathological condition that often accompanies atherosclerosis progression), we performed immunohistochemical studies of two endothelial cell-derived factors, intercellular adhesion molecule-1 (ICAM-1) and endothelial nitric oxide synthase (eNOS).

This study yielded data of collagen fiber angle distributions throughout the vessel wall in the aortas of mice with atheroprone phenotypes at different ages and on different diets. Endothelial dysfunction as a stimulus for vascular

vi

remodeling remains inconclusive. However, we conclude that the aorta displays

a distinct remodeling response in the presence of atherogenic stimuli, even in

non-lesioned areas, as observed by a shift in collagen fiber orientation.

# TABLE OF CONTENTS

# LIST OF TABLES

# LIST OF FIGURES

# LIST OF ABBREVIATIONS

apoE………………………………………………………………Apolipoprotein E

ChCs…………………………………………………….....Cholesterol crystals

DKO/KO………………………………………………….Double knockout/knockout

ECM…………………………………………………….….Extracellular matrix

eNOS/NO…………………………….....Endothelial nitric oxide synthase/nitric oxide

ICAM-1……………………………………….……….Intercellular adhesion molecule 1

IHC.................................................................... Immunohistochemistry

MMP…………………………………………….…Matrix metalloproteinase

MPM………………………………………………….….Multiphoton microscopy

PSR ........................................................................ Picrosirius red

SHG………………………………………….....Second harmonic generation

SRS…………………………………….……...Stimulated Raman scattering

SMC…………………………………………….....….Smooth muscle cell

TPEF………………………………………….Two-photon excitation fluorescence

CHAPTER 1

INTRODUCTION

Cardiovascular disease is the leading cause of death worldwide (Pagidepati et al., 2013). While the underlying causes are multifactorial, atherosclerosis is the most common (Frostegard, 2013; Pagidepati et al., 2013). Atherosclerosis is a chronic inflammatory disease characterized by endothelial dysfunction and lipid accumulation in the artery wall, which represents a significant source of morbidity and mortality in the United States (Jamkhande et al., 2014). Arteries undergo long-lasting changes in arterial structure and function, termed vascular remodeling, in response to atherosclerotic lesion development (Galis & Khatri, 2002). Vascular remodeling is defined as any lasting change in size and/or composition in an adult blood vessel. Examples of remodeling occur physiologically when there is an increase or decrease in blood flow or blood pressure, or when vascular injury occurs. As a result of one or more of these events, the distensibility of the artery is altered.

Serious complications of atherosclerosis may lead result from plaque rupture, in which lipid build up causes narrowing of the arteries and thrombus formation blocks blood supply to the heart or brain, resulting in myocardial infarction or stroke. Plaque ruptures are responsible for nearly 75% of heart attacks with a 40% fatality rate (Virmani et al., 2007). These statistics suggest the importance of studying collagen fibers and their orientation, because

1

atherosclerotic plaques are covered by a cap rich in fibrillar collagens. Information about the organization of collagen fibers can increase our knowledge regarding the mechanical behavior of the vessel and where the load is being carried.

The importance of collagen fiber angles on the mechanical behavior of the arterial wall has been well-established (Holzapfel et al., 2000; Wolinsky et al., 1969; Canham et al., 1996; Holzapfel et al., 2009), and research also shows that collagen plays a major role in disease (Hallaron et al., 1995; Lanne et al., 1992; Katsuda et al., 1992). However, there are limited published experimental studies accounting for changes in collagen fiber angles throughout the thickness of diseased (i.e. aged and/or atherosclerotic) aortas  (Holzapfel, 2000; Collins et al., 2011; Hill et al., 2012). Because the detection of collagen in the three layers of the aortic wall typically requires labeling techniques such as the use of antibodies, we used second harmonic generation microscopy (SHG) to visualize collagen fiber orientation. Collagen has birefringent properties and produces an SHG signal (Roth & Freund, 1981; Georgiou et al., 2000; Campagnola et al., 2002). This is of particular importance because, with aging and atherosclerosis, the extracellular matrix (ECM) experiences changes in the fibrous structure and content of collagen (Phillip et al., 2015).

## 1.1 Collagen Fibers

Collagen is the most abundant structural protein in mammals. It represents a heterogeneous family of extracellular matrix (ECM) proteins that is

2

generally involved in the formation of supramolecular networks (Richard-Blum, 2011). The native collagen molecule can be described as a triple helix constituted by three polypeptide chains (α chains). The central collagen domain consists of the repeating amino acid sequence glycine - X - Y, where X and Y are frequently proline or hydroxyproline, with non-collagenous domains at the terminal ends of the peptide chains (Vuorio & De Crombugghe, 1990; Van der Rest & Garrone, 1991). The secreted procollagen molecules have their non-collagenous domain removed by specific proteinases, leaving the characteristic collagen triple helices that aggregate in quarter-staggered fibrils (Schriefl, 2012).

The fibrous protein is found in extracellular matrices and connective tissues. There are at least 16 types of collagen, but 80-90% of the body's collagen consists of types I, II, and III (Lodish, 2000). These collagen molecules pack together to form long (300nm), thin (1.5nm-diameter) fibrils of similar structure (Lodish, 2000). Smooth muscle cells produce most collagens in the intima and media of vascular walls, and fibroblasts have a similar role in the adventitia (Fitzsimmons et. al., 2002). Fibrillar collagens in all layers of the vessel wall serve the same purpose, which is to help the tissue withstand mechanical loading (Lodish, 2000). Collagen fibers often align in the direction of preferred loading in the tissue (Rubbens et al., 2009). This is an example of form following function.

In humans, the fibrillar collagen family types include types I-III, V, XI, and most recently discovered types XXIV and XXVII (Exposito et. al., 2002; Koch et. al., 2003; Boot-Handford et al., 2003; Pace et al., 2003). Since the same cell can

3

synthesize different fibrillar collagens at the same time, a specific molecular mechanism is required for the recognition and discrimination of α chains during assembly of the procollagen molecule (Exposito et al., 2011). While the major types found in the vasculature are the classical fibrillar collagen types I and III (Hulmes, 2008), arterial collagen content and distribution is thought to be species-dependent (Grant, 1967).

Within atherosclerotic lesions, collagen type I is the most abundant. It is readily available for studies because it can be easily isolated. Collagen type I was also the first to be characterized among the collagens. It has been observed to form large fibers, approximately 10-500nm in diameter and several micrometers long (Lodish et al., 2000).

Assembly of these collagen fibers begins with a lag phase in which collagen molecules associate to form metastable nuclei. This stage is followed by a rapid growth phase in which more molecules accumulate around the nuclei leading to growth in fiber length and width. The final step is a plateau region in which no further growth is observed (Ward, 1986). These three phases of self-assembly of collagen fibers can be influenced by entropy (Ward, 1986).

### 1.2 Optical properties

Collagen can be visualized by methods such as polarized light microscopy (Puchtler et al., 1973; Bennett, 1950; Junqueira et al., 1979; Eberth et. al., 2009), small angle light scattering (Sacks et al., 1997), scanning confocal laser microscopy (Schrauwen et al., 2012), multiphoton microscopy (Hill et al., 2012;

4

Tsamis et al., 2013a), and second harmonic generation microscopy (Williams et al., 2005; Doras et al., 2011; Arifler et al., 2007; Watson et. al., 2015). Imaging methodologies such as second harmonic generation (SHG) microscopy, third harmonic generation, and coherent anti-Stokes Raman spectroscopy are classically used for three-dimensional structural visualization of collagen fibers with high contrast (Jemal et al.; Mueller & Fusenig, 2002; American Cancer Society, 2006; Koss, 1992). In recent years, many second-harmonic generation (SHG) experiments have been devoted to the study of collagen structures in biological tissues (Zipfel et al., 2003; Doras et al., 2011). This technique exhibits promise for biomedical assessment of tissue structure, especially in processes where the ECM is being actively remodeled (Williams et al., 2005) .

Collagen has a highly crystalline triple-helix structure that is not centrosymmetric, and the molecules are organized on the scale of the wavelength of light (Erikson et al., 2007). Because the SHG signal is intrinsic to specific structures, this technique allows for quantification of collagen fibers without physical or biochemical processing of the tissue. Individual noncentrosymmetric molecules will generate a SHG signal, but molecules arranged in a crystalline array will give a much stronger response. SHG is useful in providing information about the orientation, crystallinity, and morphology of collagen fibers (Zoumi et al, 2004; Schenke-Layland et al., 2005).

Both types of nonlinear light-matter interactions (SHG and two-photon excited autofluorescence) are utilized in the multiphoton microscopy (MPM)

5

technique (Denk et al., 1990; Williams et al., 2005; Zipfel et al., 2003) to yield high contrast and optical sectioning capabilities through relatively thick tissues.

Characterizing collagen fiber orientation throughout the vessel wall was the main focus of this dissertation and will be discussed further in the following chapters.

## 1.3 The Arterial Wall

Arteries consist of three tissue layers: the tunica intima (innermost layer), tunica media (middle layer), and tunica adventitia (outermost layer). Arteries can be classified into three types based on their properties and sizes: elastic arteries, muscular arteries, and arterioles (Moore & Dalley, 1999). The group of elastic arteries consists of the larger vessels, which are able to expand freely to maintain pulsatile blood pressures (systolic and diastolic). Among this group are the thoracic and abdominal aorta. These arteries store energy generated by the contraction of the heart; thus, this group also includes the aortic arch and its major branches and the pulmonary artery. The group of muscular arteries, also known as the distributing arteries, includes the renal, brachial, iliac, and coronary arteries. These vessels are medium in size, contain layers of smooth muscle, and serve to draw blood from the elastic arteries and branches into the arterioles. Arterioles are the smallest type of arteries and supply blood to the microcirculation, which extends from branches of the local distributing artery and leads to capillaries. Although small in diameter, they have muscular walls and are the primary site of vascular resistance.

Intimal Layer

In its simplest form, the tunica intima ('intima') of the normal artery is made of endothelial cells that are in direct contact with the blood flow. The endothelial cell layer is attached to an underlying basement membrane supported by the internal elastic lamina (an elastic connective tissue layer separating the intima and the media). This architecture allows for the exchange of nutrients and gases between the layers.

The intima is a very thin layer that exists to provide a non-clotting interface between the blood and the vessel wall (Labrosse, 2007). When the artery has not experienced any damage, the intimal layer has no structural importance to the vessel wall. It only becomes mechanically significant with arteriosclerosis and aging (Holzapfel, 2005).

Medial Layer

The tunica media ('media') is the muscular middle layer of the artery, positioned between the intimal layer and the adventitial layer. The media of arteries has more smooth muscle cells (SMCs) than the media of veins to control distribution of blood to the downstream tissues. SMCs play a role in both vasoconstriction and vasodilation, which are normal physiological functions of arteries needed to distribute blood. Among the SMCs are collagen fiber bundles and elastin (Clark & Glagov, 1979), which are the primary load-bearing components in the aortic wall. In the media, individual SMCs are surrounded by a basement membrane and are in turn embedded by the fibrillar collagens,

7

proteoglycans, and fibronectin. In a normal vessel, SMCs have a contractile phenotype, but during atherosclerotic plaque development they transition to a synthetic phenotype and begin to deposit collagen types I and III (Adiguzel et al., 2009).

Adventitial Layer

The tunica adventitia ('adventitia') consists of a network of mostly collagen type I fiber bundles (von der Mark, 1981) that display varying degrees of organization. This layer is composed of fibroblasts, connective tissue, small nerves, and vasa vasorum (a capillary network which provides the outer layers of the vessel with their blood supply) (Labrosse, 2007; Holzapfel, 2008).  Recent studies suggest that the adventitia contains stem cells that may be able to respond to arterial injury (AHA, 2011). In addition, the adventitia is in contact with surrounding tissue and may actively participate in exchange of signals and cells between the vessel wall and neighboring tissues (AHA, 2011). Thus, the adventitia plays a critical role in control of inward wall (lumen size) and outward wall remodeling responses (Smith et al., 1999; Rey et al., 2002; Korshunov et al., 2007; Tang et al., 2008).
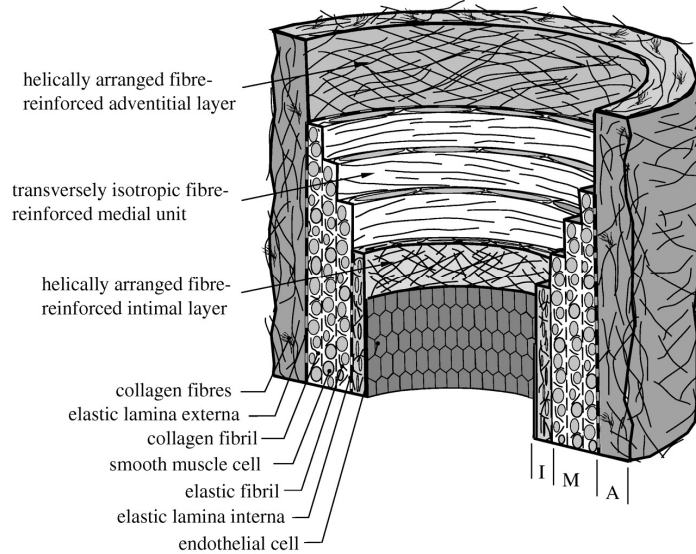
Figure 1.1: Schematic of a healthy elastic arterial wall depicting the intimal (I), medial (M), and adventitial (A) layers. Other major components of the artery wall have been labeled. Reprinted with permission from Gasser et. al., 2006.

## 1.4 Atherosclerosis

Atherosclerosis is a chronic inflammatory disease of the major arteries that develops over decades and typically worsens with aging. Its initiation is characterized by the deposition of low-density lipoprotein (LDL), infiltration of monocytes, and maturation of monocytes into LDL-engulfing macrophages in the subendothelial layer of the intima (Libby, 2015). The initial fatty streak lesions progress into plaques when smooth muscle cells penetrate the intima, leading to production of collagen fibrils and other extracellular matrix components. Advanced plaques often contain cholesterol crystals and microvessels and can rupture. Plaque rupture enables tissue factors to come in contact with blood coagulation components, triggering thrombus formation in the lumen of the

9

vessel where it can lead to flow-limiting stenoses (Libby et al., 2003; Libby et al., 2011).
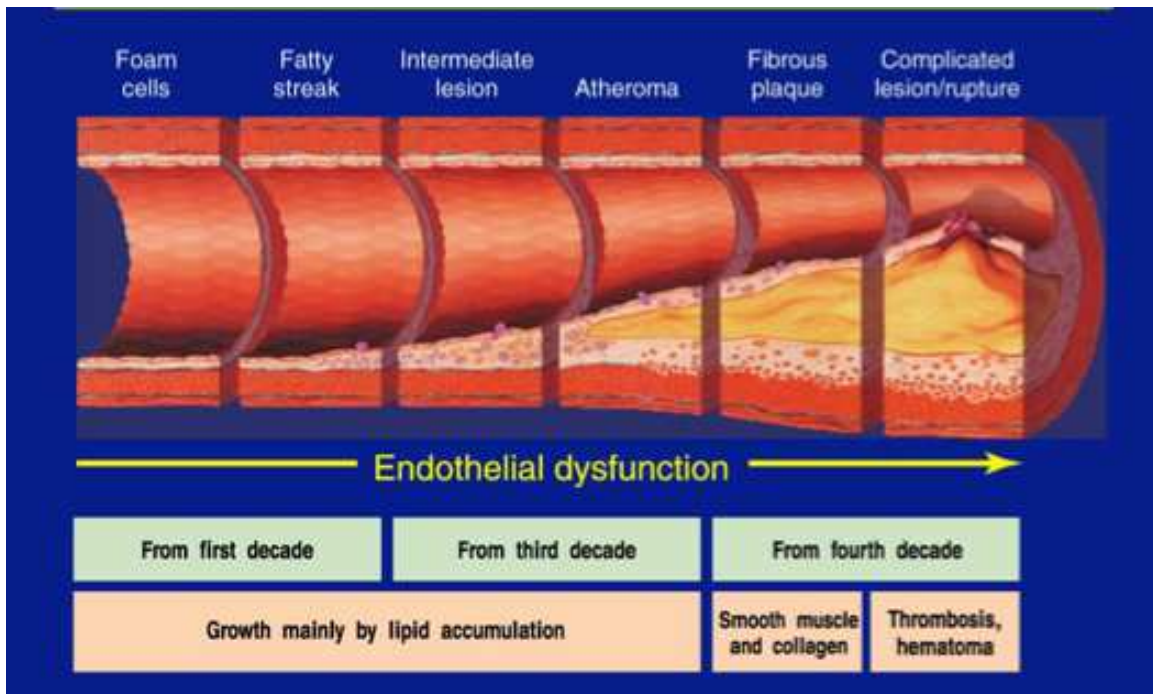


Figure 1.2: Atherosclerosis timeline showing progression of the vascular disease over a 4-decade time period. Reprinted with permission from Pepine, et. al., 1998.

From the onset of atherosclerosis throughout its progression, endothelial dysfunction remains a key problem among vascular events (Davignon, 2004). Endothelial dysfunction is a physiopathological mechanism that can be defined as an imbalance between vasoconstricting and vasodilating substances produced by the endothelium (Deanfield et. al., 2005). Endothelial dysfunction is associated with increased adhesion molecule expression and reactive oxygen species production from the endothelium (Montezano et al., 2012).

Endothelial nitric oxide synthase (eNOS) and intercellular adhesion molecule 1 (ICAM-1) are important in understanding vascular inflammation and endothelial dysfunction (Wolf & Lawson, 2012). Reduced generation of nitric oxide (NO) is considered to be a hallmark of endothelial dysfunction (Rajendran et al., 2013; Lucas, 2015). Normally, NO is released in response to flow-induced shear stress and produces vasodilation of the vessel. When NO bioavailability decreases, NO has reduced ability to inhibit atherosclerosis. eNOS is an enzyme isoform  that synthesizes NO in vascular endothelial cells (Fish & Marsden, 2006). NO produced by eNOS is essential for regulating vascular tone. ICAM-1 is a protein typically expressed on endothelial cells that plays a critical role in the firm attachment and transendothelial migration of leukocytes (Muller, 2011). ICAM-1 expression has been observed consistently in atherosclerotic plaque (Blankenburg, 2003), differing from eNOS, which is frequently reduced in atherosclerosis. Thus, the loss of eNOS is a marker of endothelial dysfunction.

**1.5 Animal Models of Atherosclerosis**

The apolipoprotein E-deficient (apoE-/-) mouse and LDL receptor knockout (LDLR-/-) mouse are widely used preclinical models that reproducibly develop hypercholesterolemia and atherosclerosis (Sánchez et al., 2014). In comparison to other mouse models of atherosclerosis, the apoE -/- has arguably been one of the most critical advances in elucidating factors affecting atherogenesis (Meir & Leitersdorf, 2004). It is particularly valued for its ability to spontaneously develop atherosclerotic lesions on a standard chow diet. By 10

11

weeks of age, these mice have foam cell accumulations in the vessel wall and delayed clearance of large atherogenic particles from circulation (Nakashima et al., 1994). ApoE-/- mice develop lesions of all phases of atherosclerosis throughout the aortic tree (Nakashima et al., 1994).

## 1.6 Matrix Metalloproteinases

Matrix metalloproteinases are a family of zinc-dependent enzymes that are capable of degrading ECM proteins. MMPs were first discovered by Jerome Gross and Charles Lapiere who observed enzymatic activity of collagen degradation in the study of tadpole tail metamorphosis (Gross, 1962). To date, many groups of MMPs have been discovered. Of interest are MMP9 and MMP12, which have different substrate specificities. MMP9 is categorized as a gelatinase, while MMP12 is a metalloelastase.

| Gene | Name | Location | Description |
|------|------|----------|-------------|
| MMP9 | Gelatinase-B | Secreted | Substrates include gelatin, collagen IV, and collagen V. |
| MMP12 | Macrophage metalloelastase | Secreted | Substrates include elastin, fibronectin, and collagen IV. |

Both MMP9 and MMP12 are thought to be important in tissue remodeling (Lagente & Boichot, 2008). Each MMP has a distinct role in plaque formation,

whether it is permitting plaque growth by facilitating cellular migration into the intima, or preventing accumulation of ECM. For example, deletion of MMP12 in the apoE KO mouse results in a decrease in the number of buried fibrous caps, while deletion of MMP9 increases the number of caps (Adiguzel et al., 2009). Both MMP9 and MMP12 mediate collagen degradation in the fibrous cap and therefore may facilitate plaque rupture. Mice with a deficiency of matrix metalloproteinases (MMPs) 9 or 12 are viable and live to be roughly the same age as wild-type mice.

## 1.7 Specific Aims

The overall goal of this project is to evaluate changes in collagen fiber organization caused by aging and/or high fat diet in atherosclerotic mouse aorta and to examine potential driving forces for vascular remodeling in this context. With aging and atherosclerosis, the extracellular matrix (ECM) experiences changes in the fibrous structure and content of collagen and elastin (Bell, 1990; Bell, 2003, AHA, 2013; Benetos, 1998). There exists a relationship between the structural proteins and the normal function of the aorta. *Therefore, investigating how the artery compensates for structural changes that occur during aging and plaque progression will lead to a better understanding of how arteries respond to mechanical loading.*

The biology of aging arteries has been well studied over the years and it has been highly documented that arteries stiffen with age. We would like to investigate how age-dependent remodeling is altered by other factors in the

13

presence of atherosclerosis. We hypothesize that changes in collagen fiber angle distribution in mouse models of atherosclerosis are initiated by endothelial dysfunction and depend on genotype (apoE KO vs. apoE MMP9 DKO vs. apoE MMP12 DKO), diet (chow diet vs. Western diet), and age (6 weeks vs. 6 months).

The following specific aims will be addressed to determine the factors influencing changes in collagen fiber angle distribution:

Specific Aim 1: To characterize 3D collagen fiber angle distribution (en-face oriented and radially-oriented) in aortic tissue in a mouse model of atherosclerosis on 6 months chow diet and 6 months Western diet using second harmonic generation microscopy. I will examine potential driving forces for vascular remodeling by comparing measurements of blood pressure and blood flow velocity to extracellular matrix composition and collagen fiber organization among groups.

Specific Aim 2: To evaluate the contribution of age-dependent changes in collagen fiber distribution by comparing collagen fiber arrangement in 6 week old mice to 6 month old mice with or without diet-induced atherosclerosis.

Specific Aim 3:  To investigate endothelial dysfunction as a stimulus for vascular remodeling and collagen fiber reorganization. I will quantitate inflammation in the

aortic tissue collected in Specific Aims 1 and 2, and measure changes in endothelial nitric oxide synthase and intercellular adhesion molecule-1 protein expression as markers of endothelial dysfunction.

# CHAPTER 2

# (SECOND) HARMONIC DISHARMONY: NONLINEAR MICROSCOPY SHINES NEW LIGHT ON THE PATHOLOGY OF ATHEROSCLEROSIS [1]

---

16

## 2.1 Abstract

There has been an increasing interest in second harmonic generation (SHG) imaging approaches for the investigation of atherosclerosis due to the deep penetration and three-dimensional sectioning capabilities of the non-linear optical microscope. Atherosclerosis involves remodeling or alteration of the collagenous framework in the affected vessels. The disease is often characterized by excessive collagen deposition and altered collagen organization. Second harmonic generation has the capability to accurately characterize collagen structure, which is an essential component in understanding atherosclerotic lesion development and progression. Previous SHG studies have examined collagen morphology, atherosclerosis burden, and cholesterol crystals. However, very few studies have attempted to quantitate differences in control versus atherosclerotic states or to correlate the application to clinical situations. This review highlights the potential of SHG imaging to directly and indirectly describe atherosclerosis as a pathological condition.

## 2.2 Introduction

Imaging methodologies such as second harmonic generation (SHG) microscopy, third harmonic generation, optical coherence tomography, and coherent anti-Stokes Raman spectroscopy (CARS) are classically used for three-dimensional structural visualization of collagen fibers with high contrast (Jemal et al. 2006; Mueller & Fusenig, 2002; American Cancer Society, 2006; Koss, 1992). In recent years, many second-harmonic generation experiments have been

17

devoted to the study of collagen structures in biological tissues (Zipfel et al., 2003; Doras et al., 2011b). This light microscopy technique exhibits promise for biomedical assessment of tissue structure, especially in processes where the extracellular matrix (ECM) is being actively remodeled (Williams et al., 2005).

Due to intrinsic contrast generated by filamentous proteins, many animal tissue structures can be imaged via SHG microscopy. These tissue structures include collagen fibrils (Watson et al., 2016; Brown et al., 2003; Stoller et al., 2002; Cox et al., 2003), microtubules (Psilodimitrakopoulos et al., 2013), interfaces between two media (Erikson et al., 2007) and the actomyosin lattice of muscle cells (Campagnola et al., 2002; Chu et al., 2004). When combined with two photon-excited fluorescence (TPEF) signals, SHG has the advantage of visualizing the presence of endogenous sources in untreated live specimens (Plotnikov et al., 2006). Most importantly, SHG imaging benefits from the use of long excitation wavelengths (near-IR), which allow for deeper penetration within a sample when compared to conventional single-photon excitation microscopy.

Historical Overview

Theodore Maiman became well known for designing a working laser when he built a pulsed ruby laser in 1960. This, the world's first laser, produced pulses of deep red (697 nm) light within the visible range (Franken et al., 1961). Shortly after, the second harmonic of the original light was discovered when it was found that shining pulses of ruby laser light through a quartz crystal produced near-ultraviolet light at 348 nm (Cox & Kable, 2006). SHG occurs when the electric

18

field of the exciting light is strong enough to deform or polarize a molecule (Gauderon et al., 2001). If the molecule is noncentrosymmetric, the resulting anisotropy creates an oscillating field at twice the frequency of the incident light, which is known as the second harmonic (Gauderon et al., 2001). Essentially SHG can be described as a coherent, nonlinear optical process in which two photons of incident light interact to give rise to a single photon having twice the frequency of the incident photons (Erikson, et al., 2007). The physical basis of this phenomenon implies that the ability to generate second harmonics of the incident light is specific to molecules that are not symmetric. Structures that are highly ordered on the molecular level are particularly strong SHG emitters because of high second order susceptibility. SHG will also take place at interfaces where there is a huge difference in refractive index, such as at metal surfaces (Gauderon et al., 2001).

SHG was first used in microscopy as long ago as 1974 but became more useful in practice in 1978 following innovations by Gannaway and Sheppard, who used a continuous-wave laser (Gannaway & Sheppard, 1978). Modern SHG imaging employs low spectral resolution, high peak power femtosecond lasers (Meyer et al., 2013). Figure 2.1 shows an example of a modular, custom-built SHG microscope for studying cutting-edge nonlinear imaging methods (Liu et al., 2011a). The microscope has the same basic requirements as a two-photon fluorescence microscope that is coupled to a pulsed infrared laser. When imaging an SHG-active molecule, the resulting anisotropy results in transmitted (or reflected) light having twice the frequency/half the wavelength of the incident light

19

and traveling in phase with it, although it commonly has a different plane of polarization. While SHG microscopy is commonly performed with detectors in the forward direction, epi-SHG has also been reported with signal collection in the backward (incident light) direction (Chen et al., 2008). In 2007, SHG microscopy was first applied to the study of atherosclerosis (Le et al., 2007). Results from those pioneering experiments are shown in Figure 2.2, which demonstrate SHG imaging of significant components of both the normal and atherosclerotic arterial wall without labeling.

Pathology

Atherosclerosis is a chronic inflammatory disease of the major arteries that develops over decades. Atherosclerosis-related diseases are the most common underlying cause of cardiovascular deaths and disability worldwide. Estimates for the United States alone suggest that 16 million people have atherosclerotic heart disease. In 2015, an estimated 1.2 million Americans were at risk for a heart attack. Despite significant advances in medicine, heart attacks and strokes due to atherosclerosis are responsible for more deaths than all other diseases combined (Lam, 2015).

The structure of the atherosclerotic aorta has been described in detail (Buck et. al., 1958). While the location of atherosclerotic plaque initiation was initially thought to be random, current consensus in the field recognizes that arterial geometry and its corresponding blood flow patterns are the primary determinants of early lesion localization (Ku et al., 1985; Caro et al., 1971; Malek,

1999). Atherosclerotic plaques are well known to develop in the carotid arteries and at aortic branch points in animal models, regions having complex flow or flow recirculation. Both thoracic and abdominal aortas from animal models of atherosclerosis have been studied (Watson et al., 2016; Isselbacher, 2005; Benvenuti et al., 2005). Atherosclerosis in the abdominal aorta may precede aneurysm and, as an indicator of systemic cardiovascular disease, may be predictive of future heart attack or stroke (Still & Marriott, 1964).

Considerable evidence from human arterial specimens and experimental models of atherogenesis supports the early involvement of the monocyte/macrophage, the most important cellular component of the innate immune response, during atherogenesis. Circulating mononuclear phagocytes attach to activated endothelial cells by leukocyte adhesion molecules. Then, specialized cytokines known as chemokines direct cell migration of monocytes into the subendothelial layer of the intima, where the monocytes later mature into low-density lipoprotein (LDL)–engulfing macrophages (Libby et al., 2009). The initial fatty streak lesions formed in this manner progress into plaques when smooth muscle cells penetrate the intima, leading to production of collagen fibrils and other extracellular matrix components. In advanced stages, lipid-rich necrotic cores, calcium deposits, and intraplaque hemorrhage are often observed. Although the most obvious impact of advanced atherosclerotic lesions is stenosis, clinical complications generally arise from plaque rupture and thrombosis, leading to myocardial infarction and stroke (Badimon et al., 2012; Osborn & Jaffer, 2013). It has been shown that the pathological behavior of

21

plaques depends not only on their size but also on their composition of collagen fibrils, lipid droplet deposits, and lipid-rich cells (Libby, 2002; Davies et al., 1993).

Fibrillar collagens are well-known matrix proteins involved in the formation of atherosclerotic lesions (Doras et al., 2011b). Collagen types I and III are the major collagen types found in atherosclerotic plaques, with type I collagen comprising approximately two-thirds of the total collagen (Mostaço-Guidolin et al., 2013). Collagen fibers are readily imaged using SHG microscopy, as described below under imaging targets. Importantly, SHG can be applied to visualize collagen fibers *in vivo* without staining.

## 2.3 Animal Models and Imaging Targets

Animal Models

The apolipoprotein E-deficient (apoE-/-) mouse and low density lipoprotein (LDL) receptor knockout (LDLR-/-) mouse are widely used preclinical models that reproducibly develop hypercholesterolemia and atherosclerosis (Ma et al., 2012; Sánchez et al., 2014; Jawien et al., 2012). In comparison to other mouse models of atherosclerosis, the apoE-/- has arguably been one of the most critical advances in elucidating factors affecting atherogenesis (Meir & Leitersdorf, 2004). It is particularly valued for its ability to spontaneously develop atherosclerotic lesions on a standard chow diet. By 10 weeks of age, these mice have foam cell accumulations in the aortic root and pulmonary root, as well as delayed clearance of large atherogenic particles from circulation (Nakashima et al., 1994). ApoE-/- mice develop lesions of all phases of atherosclerosis

22

throughout the aortic tree (Whitman, 2004; Nakashima et al., 1994; Knowles & Maeda, 2000). When examining these lesions under the SHG microscope *ex vivo*, *en face* analysis is widely used because of its speed and simplicity.

Larger animal models are better suited for preclinical studies of novel therapeutic approaches to the treatment of atherosclerosis. Pigs have an advantage over rodents as animal models of atherosclerosis due to their phylogenetic similarity to humans, comparable heart size, and large vasculature, allowing for preclinical trials of devices and interventions intended for human application (Hamamdzic & Wilensky, 2013). Anatomical similarity and development of high-risk atherosclerotic lesions make them a well-favored model for understanding atherosclerosis. There are at least four models of porcine atherosclerosis, including the diabetic/hypercholesterolemic model, the Rapacz-familial hypercholesterolemia pig, the proprotein convertase subtilisin/kexin type 9 (PCSK9) gain-of-function mutant pig model, and the Ossabaw miniature pig model of metabolic syndrome (Hamamdzic & Wilensky, 2013). Using an Ossabaw swine model, Le et al. showed that multimodal nonlinear optical microscopy that incorporated CARS, SHG, and TPEF imaging on the same platform enables a detailed study of atherosclerotic plaques, including the visualization of extracellular lipids and lipid-rich cells associated with plaque lesions (Le et al., 2007).

Other animal models of atherosclerosis include rabbits and zebrafish. A number of studies have established that adult male New Zealand white rabbits can be fed a 0.5% cholesterol diet to initiate atherosclerotic plaque progression

23

(Kolodgie et al., 1996). The rabbit model is useful because it can develop advanced lesions, but usually only with a combination of injury and hypercholesterolemia. Rabbits are well-suited for clinical imaging methods, which do not work well on the smaller mouse models of atherosclerosis. An earlier study conducted by Mostaço-Guidolin and colleagues used a NLO laser scanning microscope for TPEF, SHG, and CARS imaging of extracellular structural proteins and lipid-rich structures within intact aortic tissue obtained from Wantanabe heritable hyperlipidemic (WHHLMI) rabbits (2010). These rabbits have a hereditary defect in LDL processing equivalent to human familial hypercholesterolemia and spontaneously develop lesions without high-fat feeding. Clear differences were observed in the NLO microscopic images between healthy arterial tissue and regions dominated by atherosclerotic lesions (Mostaço-Guidolin et. al., 2010). Based on intensity changes from the multi-channel NLO images, the authors were able to differentiate between healthy regions of the vessel and those with plaque, and to show that severity of atherosclerotic lesions correlated with age in these rabbits. .

The zebrafish, while not a good model for advanced atherosclerosis, is potentially interesting in the context of SHG due to its small size and transparency in the larval stage. Researchers are able to track the development of plaques in blood vessels of zebrafish that have been fed a high-cholesterol diet (Stoletov et al., 2009). A study performed by Stoletov and colleagues used a cholesterol-enriched diet supplemented with a red fluorescent cholesteryl ester analog to visualize early events of lipid deposition in live zebrafish larvae under

24

confocal microscopy. These zebrafish constitutively expressed green fluorescent protein in endothelial cells, which enabled visualization of the vasculature (Stoletov, et al, 2009). Potentially, the entire fish could be imaged under the NLO microscope *in vivo* using SHG to visualize fibrillar collagen and muscle myosin, with MPEF imaging of intrinsic fluorophores. We have not yet seen a published description of such a study using SHG microscopy; however, the use of this transparent zebrafish model appears to be a promising method to screen for new drugs and cardiovascular imaging agents (Miller, 2009).

Imaging Targets

Thus far, SHG imaging studies have evaluated atherosclerotic lesion burden, collagen structure, and cholesterol crystals. Using multimodal NLO microscopy incorporating CARS, SHG, and TPEF imaging, significant components of arterial walls and atherosclerotic lesions such as extracellular lipid droplets, lipid-rich cells, low-density lipoprotein aggregates, collagen, and elastin can be imaged without any labeling (Le et al., 2007). The ability to probe both the structural proteins of the arterial wall and the accumulation of lipid within atherosclerotic regions makes nonlinear imaging suitable for quantitative analysis of disease progression (Lim et al., 2010). Wang et al. employed this quantitative capability to determine lipid concentration levels in various lesions of the pathological intima by examining collagen deposition within iliac arteries collected from Ossabaw pigs (Wang et al., 2009).

## Atherosclerotic Lesions and Plaque Burden

Changes in atherosclerotic plaque burden provide an experimental measure of the effectiveness of therapeutic strategies. Very few methods used *ex vivo* in mice can assess atherosclerosis burden on a volumetric (as opposed to area) basis quickly or accurately enough to process the number of samples required in preclinical studies. Sánchez and colleagues designed an easy-to-implement and relatively fast method for accurate volumetric quantification of atheroma plaque burden in mice. To visualize the lesions, the vessels were opened longitudinally for an *en face* examination and each lesion was stained with Oil Red O (Sánchez et al., 2014). Optical z-sections are taken from the top of the plaque, through the center, and at the base. After imaging, computer generated image reconstruction of the vessel is used to represent the plaque in its entirety, allowing for volume estimation. This approach can be implemented using a single excitation wavelength of a two-photon instrument to generate three confocal signals simultaneously: SHG from collagen, and TPEF from elastin and from Oil Red O-stained lipids.

Lim et al. applied three non-linear optical microscopy contrast mechanisms to detect early stage Type II/III atherosclerotic plaques in C57BL6 and apoE-/- mice (Lim et al., 2010). CARS and SHG/TPEF, respectively, were used for visualizing lipid-rich macrophages and structural organization of collagen and elastin in Western diet-fed mice. The study provided insight into the structure and composition of early stage Type II/III plaques during formation and

allowed for quantitative measurements of the impact of diet on plaque and the arterial wall (Lim et al., 2010).

Collagen Fiber Morphology and Structural Organization

Since the SHG signal is intrinsic to specific structures, this technique allows for quantification of collagen fibers without physical or biochemical processing of the tissue while permitting determination of fiber angular distribution (Yu et al., 2007). Individual noncentrosymmetric molecules will generate a SHG signal, but molecules arranged in a crystalline array will give a much stronger response. SHG is therefore useful in providing information about the orientation, crystallinity, and morphology of collagen fibers.

Collagen molecules are noncentrosymmetric and are arranged in a triple helix consisting of two alpha1 chains and one alpha2 chain to form individual tropocollagen coiled coils. Following proteolytic cleavage of the procollagen ends, five or six tropocollagen helices are packed together to form microfibrils with a diameter on the order of four nanometers. These microfibrils are then bundled together to form larger order structures, fibrils of roughly 10 to 500 nm in diameter and "fascicles" or fibers from 1-100 micrometers in diameter (Ushiki, 2002). Four types of collagens form fibrils (collagens I, II, III, and V), which differ by minor amino acid changes that affect the final conformation. Collagen I and cross-linked collagen III are the major collagen types in atherosclerotic carotid and femoral plaques (Bode et al., 1999). Only a small amount of collagen type IV is found in atherosclerotic lesions. Collagen IV forms sheets in basal laminae, but

27

type I is of most interest because it is very important as a structural component of soft tissues, including the fibrous caps of atherosclerotic plaques.

Traditionally, the most popular methods to investigate tissue collagen organization have included conventional histochemistry with imaging by brightfield or cross-polarized light, immunohistochemistry, and electron microscopy. However, these techniques require tissue processing and sample preparation methods, which can lead to undesirable alterations of the extracellular matrix and damage tissue structure permanently. Several other imaging modalities exist such as magnetic resonance imaging and small angle X ray scattering, but some of these alternatives suffer from low chemical specificity and/or low spatial resolution. In conventional histology, collagen matrix is often evaluated after staining tissue sections using Masson's Trichrome or similar combinations of stains to differentiate collagen from elastic fibers. However, processing for histological examination can cause artifacts, such as increased or decreased interstitial volume. As a result, the natural alignment and spatial distribution of extracellular matrix proteins may be poorly defined.

The unusual structure of type I collagen makes it an effective generator of second harmonics, which has been appreciated for over 20 years (Roth & Freund, 1981). The SHG signal is wavelength independent over a wide range of wavelengths in the infrared region (Georgiou et al., 2000; Cox et al., 2003) and there have been reports of differences between the signal of normal and experimentally damaged collagen (Kim et al., 2000). An advantage to using SHG is its capability to distinguish collagen fibers from elastin fibers without staining or

28

embedding specimens. Changes in collagen fibril morphology such as fibril length, fibril thickness, or fibril alignment can then be tracked by texture analysis of SHG images as described below (Mostaço-Guidolin et al., 2013).

Over the past decade, methods to accurately characterize the tissue composition and morphology (Meyer et al., 2013) using SHG have emerged. SHG has become a useful tool for direct visualization of extracellular collagen in bulk tissues without invasive tissue staining  (Mostaço-Guidolin et al., 2013). For tissue imaging, SHG does not induce photo bleaching because there is no net energy absorption by the sample (Palero et al., 2007; Mostaço-Guidolin et al., 2013). SHG, unlike TPEF, is a nonlinear optical scattering process which does not require absorption of photons followed by fluorescence emission. The scattered photons are coherent with the incident ones. Thus, SHG provides an important tool for imaging tissue *in vivo* or in sections (Erikson et al., 2007) because it does not heat the sample and causes less damage to the tissue. The capabilities of this technique led Chen and colleagues to apply it to the tendon-muscle junction of chicken wing where it was discovered that different sources of SHG (for example, collagen and myosin) can be separated in an SHG image. The epi-illuminated microscope configuration shows potential in differentiating molecular species responsible for SHG signals during in vivo studies (Chen et al., 2010). Doras and associates have used polarization state studies of SHG to trace atherosclerotic lesions in mice (Doras et al., 2011b). Their results contradicted previous studies which stated that the observed depolarization was linked to collagen denaturing. Doras et al. suggested instead that atherosclerosis

brings structural damage reflected in the spatial coherence of the collagen but that it does not affect the triple helix structure of collagen; that is, only the spatial distribution of collagen in tissue is disordered (Doras et al., 2011b).

Despite the ease of imaging collagen fibers by SHG, most published works rely on SHG to describe collagen organization without using quantitative measures (Mostaço-Guidolin et al., 2013). However, Mostaço-Guidolin, Chu, and their associates provided quantitative studies that effectively describe aspects of collagen fibril architecture. Mostaço-Guidolin and colleagues provided a quantitative study using SHG images acquired from aortic segments of the atherosclerotic rabbit (2011). These researchers presented an image analysis method that was capable of quantifying morphological changes in collagen fibril organization that would be ideal for tracking collagen remodeling resulting from atherosclerosis. The novelty was achieved by applying a combination of texture analysis based on first order statistics (FOS) and second-order statistics such as gray level occurrence matrix (GLCM) to extract SHG image features associated with structural and biochemical changes in tissue networks. The method proved to be >90% accurate in classifying SHG imaged collagen from atherosclerotic arteries (Mostaço-Guidolin et al., 2013). Chu et al. reliably estimated collagen fibril thickness noninvasively by SHG forward/backward ratio (Chu et al., 2007). Quantitative approaches pioneered in these studies can be used to further investigate collagen fibril changes caused by pathological conditions.

Cholesterol Crystals

The accumulation of lipids in the arterial wall results in the formation of lipid-rich plaques, a prominent feature of atherosclerosis (Virmani et al., 2006). Lipid accumulation in plaques has motivated quantitative evaluation of cholesterol and cholesteryl esters. Cholesterol crystals are important in atherosclerosis because studies suggest that these crystals are capable of inducing inflammation, a proven hallmark of atherogenesis (Suhalim et al., 2012). Cholesterol crystals are capable of perforating cell membranes and the fibrous cap of the plaque, which could activate apoptosis and cause plaque rupture (Abela, 2010). While cholesterol crystals have a strong stimulated Raman scattering (SRS) signal, they also exhibit a strong SHG signal which indicates that these structures are non-centrosymmetric (Suhalim et al., 2012). Suhalim et. al. produced the first published study using SHG to image cholesterol crystals in atherosclerotic specimens (Figure 2.3).

## 2.4 Recent Advances and Future Research Goals

In most recent published work, collagen SHG images were presented to describe empirical observations that were linked to a particular pathological condition, but few studies exist that quantitate collagen organization. To date, quantitative collagen analysis has largely relied on pixel-counting applied to histological images of tissue (Rawlins et al., 2006; George et al., 1995). Several more sophisticated quantitative approaches to characterize changes in collagen architecture have been pioneered by Mostaço-Guidolin, Chu, and their

associates as described above. Our lab has recently used SHG imaging to compare collagen fiber organization in apoE knockout (KO) and apoE matrix metalloproteinase-12 (MMP12) double knockout (DKO) mice as a function of diet, mouse strain, location (abdominal vs. thoracic aorta), and radial position (depth) in the vessel wall. We performed multivariate statistical analysis using collagen fiber angle absolute value as a quantitative measure (Watson et al., 2016). Using this approach, we have characterized collagen fiber angle distribution throughout the thickness of the mouse aorta. Our results indicate that the aortas of both apoE KO and apoE MMP12 DKO mice fed a Western diet for 6 months have significantly lower (more circumferential) absolute collagen fiber angles compared to mice on a chow diet at a similar age. This difference coincides with the development of extensive aortic atherosclerosis, suggesting that differences in collagen fiber angle are part of the vascular remodeling process (Watson et al., 2016).

The SHG and statistical approaches described in Watson et al., 2016 should also be useful in comparing collagen fiber organization in fibrous caps under different treatment conditions designed to reduce the risk of plaque rupture. While we took advantage of the fact that the mouse aorta is thin enough (less than 200 micrometers) that the entire wall thickness can be imaged in en face specimens, a similar approach could easily be applied to radial sections of vessels from species having thicker artery walls. We believe that important insights could be gained by incorporating SHG in studies of arterial aging with and without disease. Such investigations would lead to a better understanding of

the effect of aging during atherosclerosis development. Changes in the biomechanical properties of arteries associated with both aging and atherosclerosis have been well documented, but there remains much that is not understood regarding how the ECM remodels while maintaining normal vascular function during these states. It is expected that collagen fiber architecture will be reorganized during both processes, but possibly in different orientations based on the local stress state of the vessel wall. A quantitative study that provides data on changes in individual tissue layers due to aging with or without atherosclerosis is needed to better understand the pathology as well as the timeline of the disease.

**2.5 SHG Advantages and Disadvantages in Assessing Atherosclerosis**

This paper has discussed SHG as a powerful tool for tracking alterations in normal arterial structure that take place during atherosclerotic lesion progression. SHG microscopy provides a simple yet elegant approach to describe collagen morphology in atherosclerotic lesions. It can be used to determine collagen fiber thickness (Chu et al., 2007), length (Mostaço-Guidolin et al., 2013), and alignment (Watson et al., 2016). Furthermore, it has been shown that SHG is useful in quantifying plaque composition (Le et al., 2007) and identifying areas with plaques that are vulnerable to rupture risk. Currently, collagen is the most widely studied aspect of atherosclerosis using SHG imaging techniques, but this technique does not currently possess the ability to distinguish between different types of fibrillar collagens. Antibodies are needed to

33

supplement SHG studies when the specific molecular identity of collagen fibers is of interest.

One disadvantage of SHG microscopy is that the structures of interest must be noncentrosymmetric. Otherwise, SHG must be paired with additional nonlinear imaging microscopies such as MPEF or CARS, which have also been shown to be very effective. Noncentrosymmetric structures viewed using SHG do not require staining and will not photobleach. SHG is superior to conventional imaging techniques because the use of near-IR lasers allows for imaging at greater penetration depth in biological tissues; with appropriate z-axis control, this feature permits optical sectioning of thick samples. In a clinical setting, we look forward to catheter-based SHG technologies to aid assessment of fibrous cap structure and stability in human atherosclerotic lesions.

## 2.6 Conclusion

While interest in biomedical applications of SHG microscopy has increased in recent years, multimodal nonlinear imaging approaches have not yet been incorporated into systems that are simple and robust enough for clinical use. Development of such systems is an exciting area for future directions of research. It would be beneficial to advance this technology to improve healthcare, given that current studies suggest that changes in spatial coherence of collagen may provide valuable information about damage caused by diseases such as atherosclerosis. Multimodal nonlinear optical imaging of plaque composition also allows identification of atherosclerotic regions that are

vulnerable to rupture risk. The nonlinear optical microscope has demonstrated that it has characteristics superior to other microscopes such as label-free molecular imaging of atherosclerotic lesions with 3-dimensional submicrometer resolution. This means that it has potential application to the evaluation of atherosclerotic plaques, determination of their rupture risk, and design of individualized drug therapy based on plaque composition.
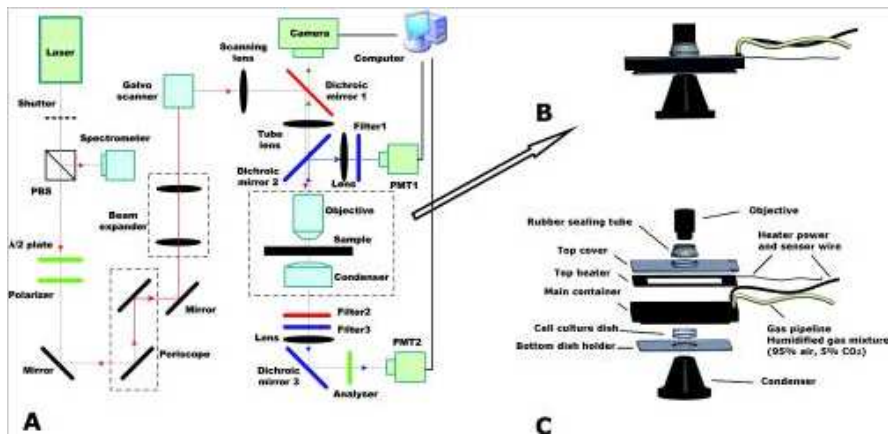
Figure 2.1**:** Schematic of a hybrid TPEF-SHG microscope with an on-stage incubator: (a) Schematic of the imaging system; (b) Location of the on-stage incubator; (c) Components of the on-stage incubator. Modified from Liu, et al., 2011.
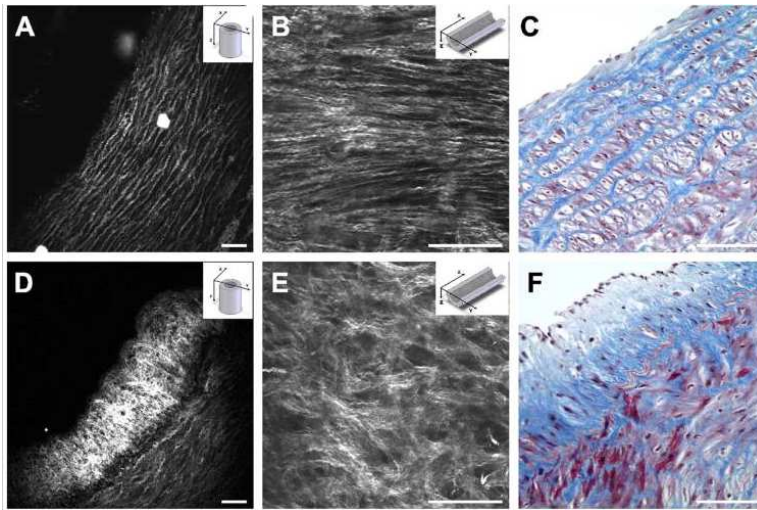
Figure 2.2: SHG and histology images of healthy versus atherosclerotic iliac arteries from Ossabaw pigs. (a) Cross sectional and (b) luminal views of collagen in a healthy arterial wall. (c) Histology of a healthy iliac artery stained for collagen (blue) using Masson's trichrome stain. (d) Cross sectional and (e) luminal views of collagen in an atherosclerotic artery. (f) Histology of an atherosclerotic artery stained for collagen using Masson's trichrome stain (blue). SHG images were acquired with a 20× air objective. Histology images were acquired with a 40× air objective. Scale bars: 75µm.
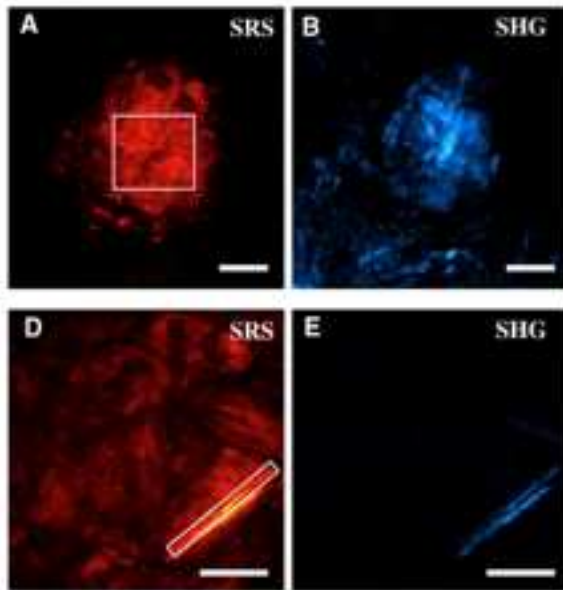
Figure 2.3: SRS (A & D) and SHG (B & E) identification of ChCs in atherosclerotic plaques of an apoE -/- mouse. Of interest, B and E images show that bright spots in the SHG images were indeed generated through second-harmonic activity of the molecules. Scale bars = 25μm.

# CHAPTER 3

# COMPARISON OF AORTIC COLLAGEN FIBER ANGLE DISTRIBUTION IN MOUSE MODELS OF ATHEROSCLEROSIS USING SECOND-HARMONIC GENERATION (SHG) MICROSCOPY[2]

### 3.1 Abstract

Characterization of collagen fiber angle distribution throughout the blood vessel wall provides insight into the mechanical behavior of healthy and diseased arteries and their capacity to remodel. Atherosclerotic plaque contributes to the overall mechanical behavior, yet little is known experimentally about how collagen fiber orientation is influenced by atherogenesis. We hypothesized that atherosclerotic lesion development, and the factors contributing to lesion development, leads to a shift in collagen fiber angles within the aorta. Second-harmonic generation microscopy was used to visualize the three-dimensional organization of collagen throughout the aortic wall and to examine structural differences in mice maintained on high-fat Western diet versus age-matched chow diet mice in a model of atherosclerosis. Image analysis was performed on thoracic and abdominal sections of the aorta from each mouse to determine fiber orientation, with the circumferential (0°) and blood flow directions (axial ±90°) as the two reference points. All measurements were used in a multiple regression analysis to determine the factors having a significant influence on mean collagen fiber angle. We found that mean absolute angle of collagen fibers is 43° lower in Western diet mice compared with chow diet mice. Mice on a chow diet have a mean collagen fiber angle of ±63°, whereas mice on a Western diet have a more circumferential fiber orientation (~20°). This apparent shift in absolute angle coincides with the development of extensive aortic atherosclerosis, suggesting that atherosclerotic factors contribute to collagen fiber angle orientation.

40

## 3.2 Introduction

Acute cardiovascular events such as myocardial infarction and stroke are frequently the result of atherosclerotic plaque rupture, which has become a leading cause of death globally (Anderson & Chu, 2007; Tunstall-Pedoe, 2006). Atherosclerosis-related diseases accounted for 68% of cardiovascular disease deaths in 2010 (NIH and NHLBI, 2012). Development of atherosclerosis leads to well-documented molecular and structural changes within the intimal and medial layers of the artery. Studies evaluating differences in collagen fiber orientation associated with atherosclerosis are needed to better understand how the artery maintains mechanical homeostasis after plaque formation.

Collagen is a major fibrillar protein in the extracellular matrix (ECM) that provides mechanical strength to many tissues. Organization of the collagen matrix and orientation of collagen fibers within the matrix can vary significantly for different tissue types (Arifler et. al, 2007) and these characteristics dramatically influence the anisotropic behavior of collagenous tissues. Accordingly, changes in collagen content and organization play a significant role in various vascular pathologies such as aneurysm development (Hellenthal et al., 2009; Alexander, 2004) and atherosclerosis (Levene & Poole, 1962). Previous studies have suggested that matrix metalloproteinases (MMPs), a family of proteolytic enzymes that degrade extracellular matrix proteins, are essential in vascular remodeling (Raffetto & Khalil, 2008; Kuzuya & Iguchi, 2003; Galis & Khatri, 2002). In particular, MMP12 plays a role in arterial stiffening during vascular remodeling (Liu et al., 2012).

41

Collagen can be visualized by many methods. In recent years, second-harmonic generation (SHG) experiments oftentimes have been used to study collagen structures in biological tissues (Zipfel et al., 2003; Doras et al., 2011a). This technique offers many advantages for biomedical assessment of tissue structure, especially in processes where the ECM is actively remodeled (Williams et al., 2005). The use of long excitation wavelengths (near-IR) in SHG systems allows for deeper penetration within a sample when compared to conventional single-photon excitation microscopy. Thus, SHG microscopy permits optical sectioning through relatively thick tissue layers, including the mouse aortic wall. Because the SHG signal is intrinsic to specific structures, this technique allows for both quantification of collagen fibers without staining and determination of fiber angular distribution in mouse aortic specimens.

Previous work has been devoted to the study of fiber directions in different arteries subjected to unique environmental conditions (Finlay et al. 2002; Holzapfel et al., 2002; Rhodin, 1980; Wicker et al., 2008; Gasser et al., 2006; Hill et al., 2012; Collins et al., 2011). Fiber reorganization is likely an adaptive process optimized to restore tissue homeostasis, which is perturbed in animal models of atherosclerosis. However, analysis of the collagen fiber angle distribution has not been well characterized in an atherosclerosis mouse model. In this work, the authors have added to previous findings by evaluating collagen fiber orientation in an atherosclerotic mouse model, where microstructural changes in collagen arrangement are associated with atherosclerosis. We reasoned that plaques within the aorta cause a change in collagen fiber

www.manaraa.com

orientation in non-lesioned areas to accommodate arterial wall injury. In addition, we hypothesized that collagen fiber orientation differs between the thoracic and abdominal aorta, since previous studies have reported differences in biomechanical behavior of these two regions (Guo & Kassab, 2003; Wolinsky & Glagov, 1969). Biomechanical differences have implications for vascular disease localization and progression. For example, in humans the abdominal aorta is particularly susceptible to aneurysm development (Xu et. al. 2001).

In this paper, we report the use of a SHG imaging technique to quantify the collagen fiber distribution and alignment in a mouse model of atherosclerosis in lesion-free regions of the vessel wall. We employ a novel statistical analysis to study 3D fiber distribution and provide details on differences in collagen fiber orientation in mice on chow diet vs. Western diet.

### 3.3 Materials and Methods

To promote atherosclerotic lesion formation within the aorta, apolipoprotein E (apoE) knockout (KO) (Nakashima et al., 1994) and apoE matrix metalloproteinase-12 (MMP12) double knockout (Luttun et al., 2004) mouse strains were fed a high-fat Western diet (42 kcal% fat) for 6 months. Control mice were age-matched and maintained on a regular chow diet. The apoE KO mice are susceptible to atherosclerosis due to a genetic defect in their ability to clear circulating plasma lipoproteins. In addition, mice lacking the MMP12 gene have a genetic deficiency in their ability to degrade elastin.

43

Sample Preparation

All mice were handled in compliance with protocols approved by the University of South Carolina Institutional Animal Care and Use Committee. Mice were ethically euthanized by carbon dioxide asphyxiation and then perfused through the left ventricle with heparinized normal saline for five minutes at physiological pressure, followed by pressure perfusion fixation for 10 minutes with 10% neutral buffered formalin. Aortas were harvested from apoE KO and apoE MMP12 DKO mice (n=5 each strain). Under a dissecting microscope, each aorta was opened longitudinally for en face examination of the collagen fibers. Non-lesioned areas were chosen in the thoracic aorta, which was sampled at the level of the fourth intercostal arteries, and the abdominal aorta, which was sampled from the infrarenal area (Figure 3.1A). The samples were flattened to a slide and labeled according to the mean orientation of blood flow for each specimen (Figure 3.1B-3.1D).

Second-harmonic generation microscopy

To image collagen fibers, we used a hybrid two photon excitation fluorescence (TPEF)-SHG microscope previously described (Liu et al., 2011). The luminal surface was validated using Hoechst staining to detect endothelial cell nuclei with TPEF microscopy. The SHG microscope was used to perform optical sectioning of each sample, making it possible to visualize collagen fibers throughout the vessel wall thickness. The SHG signals were collected from the forward direction through an Olympus 1.4 NA oil immersion condenser (Liu H et

44

al., 2011; Liu H et al., 2013). The microscope's XYZ stage was controlled through three orthogonally mounted motors to obtain image stacks from four regions of each sample by moving the stage 100µm in each direction while optically slicing the vessel wall from top to bottom at 60X. The area in pixels for each image was 512x512 pixels with the actual calibrated image being 176x176 microns.

Semi-Automated Image Analysis

The individual, local fiber orientations were determined in the Z-θ plane (Figure 3.1E). To quantify collagen fiber orientation, we first define a coordinate system. The coordinate system used in this work is shown in Figure 3.1. Here, Z is along the axial/flow direction and θ is along the circumferential/hoop direction in the specimen. The fiber angle relative to the θ-direction is denoted by ξ, with +ξ defined as the CCW angle from θ towards Z. Thus ξ = 0° corresponds to the circumferential direction (+θ) and ξ = 90° corresponds to the flow direction (+Z) in the artery. To determine ξ for each specimen, we used an analytic protocol for automatic angle recognition as previously described (Wicker et al., 2008; Tang et al., 2014). Continuity software (version 6.4b, http://www.continuity.ucsd.edu/Continuity) was used to trace the curvature of each fiber, based on an intensity gradient algorithm. Each image of the stack was analyzed and provided a 3-D histogram showing distribution of local fiber angles throughout the depth of the tissue.

45

Statistical Analysis

For this study, we used a mixed model to analyze fiber angle distribution as a function of four variables, using the R package "lme4" (Bates et al., 2014). The four variables were diet, strain, location, and through-thickness position. The average absolute angle was estimated by $\xi = C_0 + C_1(\text{diet}) + C_2(\text{anatomical location}) + C_3(\text{mouse strain}) + C_4(\text{through-thickness position})$, where the Cs are the regression parameters. To account for the regional variability of the artery, we investigated through-thickness position as a categorical variable. Thus, $\xi$ is a function of radial position in the artery, $\xi = \xi(r)$, with the radius varying from the inside, $r_i$, to the outside, $r_o$. Thus, the three radial regions are $r_i < r_1 < r_i + t/3$; $r_i + t/3 \leq r_2 < r_i + 2t/3$; $r_i + 2t/3 \leq r_3 < r_o$, where t is the average thickness of the vessel wall. Variables with $P < 0.05$ were considered statistically significant.

## 3.4 Results

Collagen fiber organization in chow diet vs. Western diet mice

Figure 3.2 provides representative second-harmonic generation images of aortic tissue segments from chow diet-fed and Western diet-fed mice used in this study. The collagen fibers of the chow diet mice are aligned at an average angle $\xi \approx 63°$ relative to the circumferential, whereas the Western diet specimens show more circumferentially aligned collagen fibers (average angle $\xi \approx 20°$). Thus, the data shows that the mice on a Western diet have collagen fibers that are more closely aligned with the circumferential direction than mice fed a chow diet for the same duration.

Constructed 3D histograms of collagen fiber distribution across aortic wall

Figure 3.3 provides an illustration of representative 3D histograms of collagen fiber angle distribution for each mouse strain on chow diet and Western diet. Zero degrees is the circumferential direction. Figures 3.3 A and C present the distribution of the fiber angles in thoracic aorta specimens from each strain, and Figures 3.3 B and D present equivalent information for abdominal aorta specimens. The 3-D histograms reflect image stacks for one individual mouse on each diet. The relative radial position, $\beta = (r - r_i)/t$, in each histogram represents the position within the arterial wall, with $\beta = 0$ corresponding to the endothelial surface and $\beta = 1$ to the outer boundary of the adventitia. Note that $\beta$ accounts for individual variations in tissue thickness among samples, since t can be varied to match the specimen geometry, with each $\beta$ corresponding to one slice of the image stack.

Statistical Analysis

Figure 3.4 shows a boxplot comparing the median, first, and third quartiles of collagen fiber angle observations for Western diet and chow diet fed mice of each strain. Here, $\xi$ is the response variable, which is the absolute value of the collagen fiber angles. In the multiple regression model, we studied whether the four factors diet, anatomical location, strain, and $\beta$ contributed to angle distribution variability. Table 3.1 summarizes the contribution of each statistically significant factor to the overall variability in $\xi$, as well as the 95% confidence interval for each coefficient. For both apoE KO and apoE MMP12 DKO mice,

multiple regression analysis showed a significant difference in average absolute fiber angle, $|\xi_{avg}|$, between mice on a chow diet vs. mice on a Western diet. A summary of mean values and standard errors for each statistically significant regression parameter is provided in Table 3.1.

As shown in Table 3.1, there was no significant difference in $|\xi_{avg}|$ between mouse strains. Abdominal location within the aorta (thoracic vs. abdominal) and relative radial position within the specimen had small, but significant, effects on $|\xi_{avg}|$. Thoracic aorta specimens had average fiber angles, $\xi_{avg}$, that were 0.84° lower (95% confidence interval [-1.00°, -0.67°] than abdominal specimens. In addition, statistical analysis showed that the outer third of the vessel ($2/3 < \beta < 1$) had slightly greater fiber angles (+0.3°, 95% confidence interval [+0.08°, +0.50°] compared to the inner two-thirds of the vessel ($0 < \beta < 2/3$). This observation is placed in context with previous work in the following section.

### 3.5 Discussion

It is important to study collagen fiber angles to better understand the anisotropic behavior of arteries. Collagen fibers have preferred directions associated with the mechanical stresses on the tissue (Holzapfel, 2000), and investigating fiber orientation and arrangement in disease states such as atherosclerosis demonstrates adaptability to maintain homeostasis. Although there is much literature published on collagen fiber angles in aneurysms and in healthy arteries (Collins et al., 2011; Hill et al., 2012; Gasser et al., 2006; Guo &

48

Kassab, 2003), we are the first to report differences in collagen fiber angles due to a diet linked to atherosclerosis.

Changes in collagen fiber angle are important for understanding the capability of the artery to remodel after arterial lesion development. Structure-based material constitutive models incorporate the mean collagen fiber angle as a geometric parameter that can be identified based on mechanical behavior (Holzapfel, 2000). Originally these models assumed a single value of the angle for each fiber family, but more sophisticated recent material models take into account fiber dispersion (Holzapfel et al., 2015; Li & Robertson, 2009; Driessen et al., 2008). With regard to findings, our experimental results demonstrate a significant dispersion of collagen fibers around the mean fiber angle.

With regard to the mean fiber angle, the predicted angles of collagen fibers of a representative carotid artery from a rabbit using a two-fiber-family constitutive model are reported to be 29° in the media and 62° in the adventitia (Holzapfel, 2000). Our data for the adventitial layer (outer 1/3 of vessel) of the normal mouse thoracic aorta reveals a mean fiber angle (62.3°) similar to that predicted for the rabbit carotid adventitia. However, statistics reported in the previous section show that our measurements indicate little difference between the mean fiber angle in the medial layer (62.0°) and that in the outermost layer.

We chose to compare the thoracic and abdominal portions of the mouse aorta because the abdominal aorta is more susceptible to aneurysm formation in humans. Aneurysm development can be regarded as an extreme case of vascular remodeling, which would be expected to have a major effect on collagen

49

fiber arrangement.  Using a structure-based constitutive model, Collins et al. (2011) reported that the predicted mean fiber angle for normal (wild type) mouse infrarenal abdominal aorta is 39° with respect to Z direction (51° relative to θ direction) and Collins et al. (2012) show a mean collagen fiber angle in an aneurysmal aorta to be 41° with respect to the Z direction (49° relative to θ direction). Our observed mean fiber angle for the infrarenal abdominal aortic media of 62.8° in chow diet-fed mice is higher than the predicted value based on the four fiber-family model.  However, we examined collagen fiber angles in mice which were much older than those used by Collins, et al. (7-8 months vs. 2-3 months). These investigators found only subtle mechanical differences between the suprarenal and infrarenal abdominal aortas (Collins et al., 2011). We show that there are small but significant differences between the average absolute angles based on anatomical location (thoracic vs. abdominal aorta). On average, the mean collagen fiber angle in the thoracic aorta is 0.84° less than that in the abdominal aorta. Our data support the hypothesis that there is a small but significant difference in collagen organization between anatomical locations, even in mice with no significant vascular pathology.

In this study, we focused on differences due to atherosclerosis and showed that Western diet feeding results in an apparent shift in average collagen fiber angles, with a mean difference of ≈ 43° (Figure 3.4). This result could indicate that differences in collagen fiber orientation are an important part of the vascular remodeling process. The exact mechanism responsible for this shift in collagen fiber orientation is unknown and thus requires additional study.

The Continuity image analysis protocol is effective for investigating collagen fiber angle differences within the extracellular matrix. We show that this image analysis method can be used for atherosclerosis and vascular remodeling studies to compare differences in aortic collagen fiber organization in mice on a chow diet or Western diet. Collectively, SHG imaging techniques and Continuity provide a plethora of data. Since there was no standard approach to interpret three-dimensional fiber angle distributions, we developed a new statistical approach to analyze the data. Based on the statistical analysis, our data indicates that the aortas of both apoE KO and apoE MMP12 DKO mice fed a Western diet for 6 months have significantly lower mean collagen fiber angles than age-matched mice maintained on a chow diet.

### 3.6 Limitations of the Study

A limitation of this study is that we have not taken advantage of TPEF microscopy for viewing elastin in the same specimens. In addition, we report average local fiber orientations and do not account for the waviness of individual collagen fibers within this study.

We only considered collagen fiber angle distribution in en face specimens. Data that compares en face collagen fiber angles in the unloaded state to the collagen fiber angles in tubular intact vessels subjected to physiological loading is limited. However, we do not believe that en face images versus ring tissue images would render different fiber angles because the Z-θ plane remains the same. Partial confirmation of this conjecture was reported by Hill and colleagues

51

(Hill et al., 2012). They noted that fiber orientation is the same in three mechanical models where the investigators idealized collagen distribution as planar.

Our research interest was centered on differences in collagen fiber angle distribution that coincide with atherosclerotic lesion formation within the aorta. There is a need to understand differences between the thoracic and abdominal aorta because of the common association of atherosclerosis with abdominal aortic aneurysm. Finally, we focused on differences in mouse strains (apoE KO and apoE MMP12 DKO mice) to evaluate the contribution of matrix metalloproteinases to collagen fiber alignment and we did not find any significant differences with the knockout of MMP12.

## 3.7 Conclusions

Our data indicate that the aortas of both apoE KO and apoE MMP12 DKO mice fed a Western diet for 6 months have significantly lower (more circumferential) absolute collagen fiber angles compared to mice on a chow diet at a similar age. This difference coincides with the development of extensive aortic atherosclerosis, suggesting that differences in collagen fiber angle are part of the vascular remodeling process.
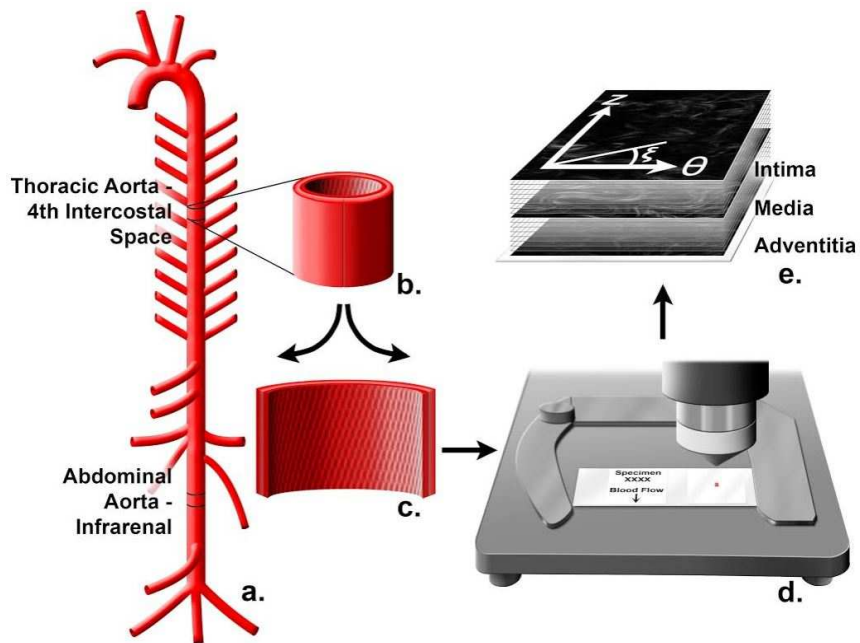
Figure 3.1: A) Depiction of the aortic tree denoting sampling areas, intercostal (thoracic) and infrarenal abdominal areas. B) and C) Segment of aorta before and after longitudinal cutting. D) Images are flattened to a slide and viewed on SHG microscope. E) The resulting data is a stack of images.

Figure 3.2: Representative second-harmonic generation images of thoracic aorta of apoE KO mouse on a chow diet (left) versus thoracic aorta of apoE KO mouse on Western diet (right). Images were captured in the media layer. Bars = 10 μm. Circumferential direction is denoted by θ, with + ξ positive clockwise and denoting the measured fiber angle.

Figure 3.3 A: Representative three-dimensional (3D) histograms of fiber angle distributions as a function of relative distance from the lumen in the thoracic aorta of apolipoprotein E knockout (apoE KO) mice on a chow diet and on W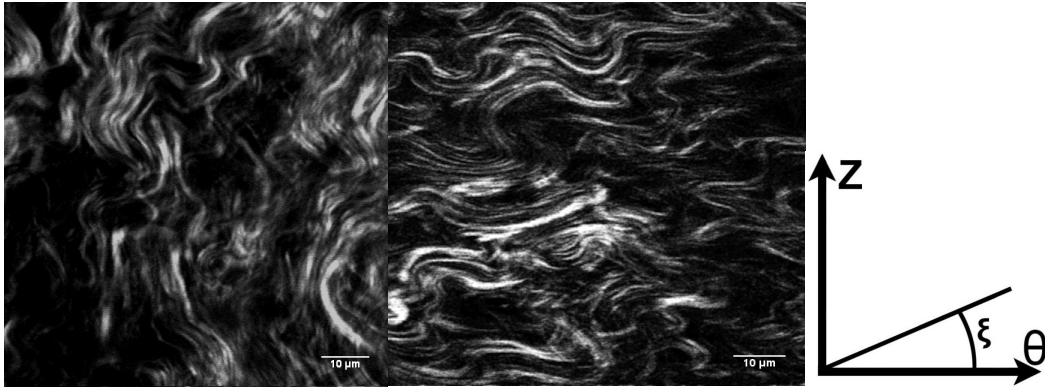estern diet for 6 months. B: Representative 3D histograms of fiber angle distributions as a function of relative distance from the lumen in the abdominal aorta of apoE KO mice on a chow diet and on Western diet for 6 months. C: Representative 3D histograms of fiber angle distributions as a function of relative distance from the lumen in the thoracic aorta of apoE matrix metalloproteinase-12 double knockout (MMP12 DKO) mice on a chow diet and on Western diet for 6 months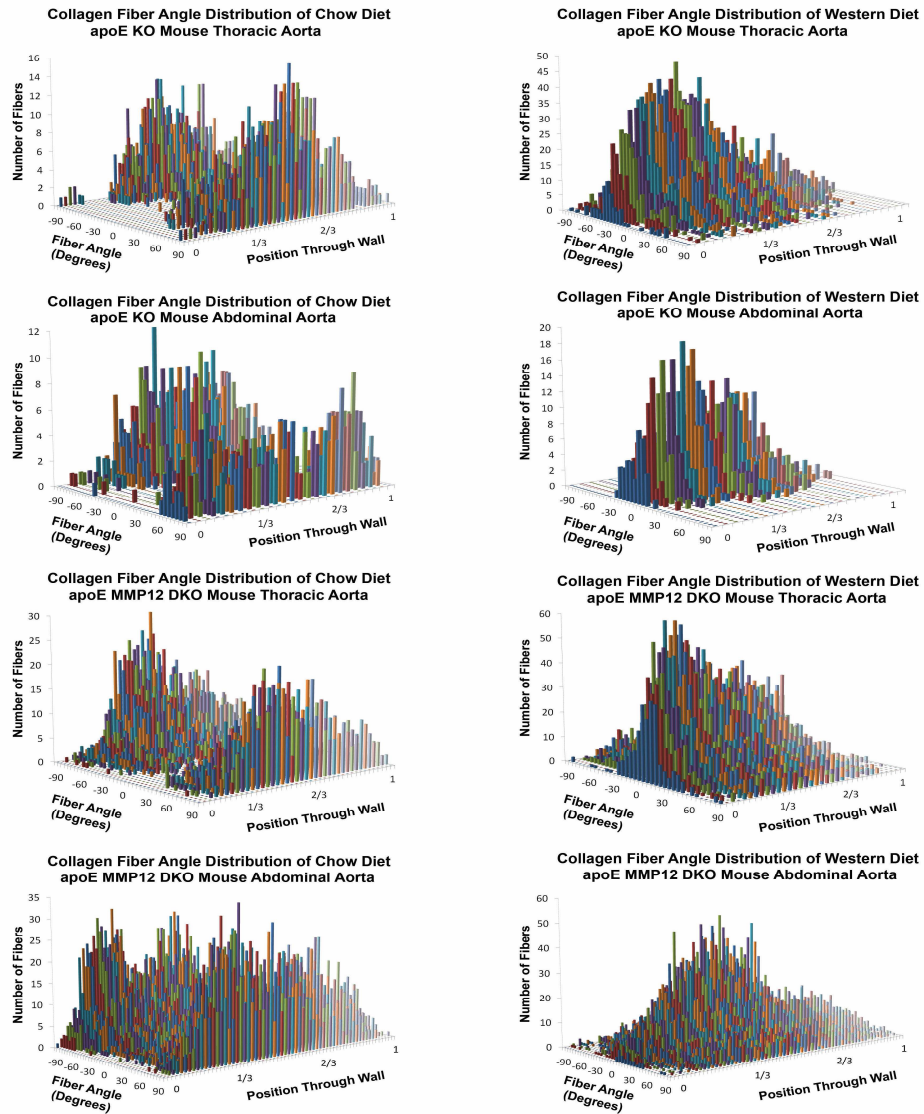. D: Representative 3D histograms of fiber angle distributions as a function of relative distance from the lumen in the abdominal aorta of apoE MMP12 DKO mice on a chow diet and on Western diet for 6 months.

55

**Boxplot of Absolute Angles**
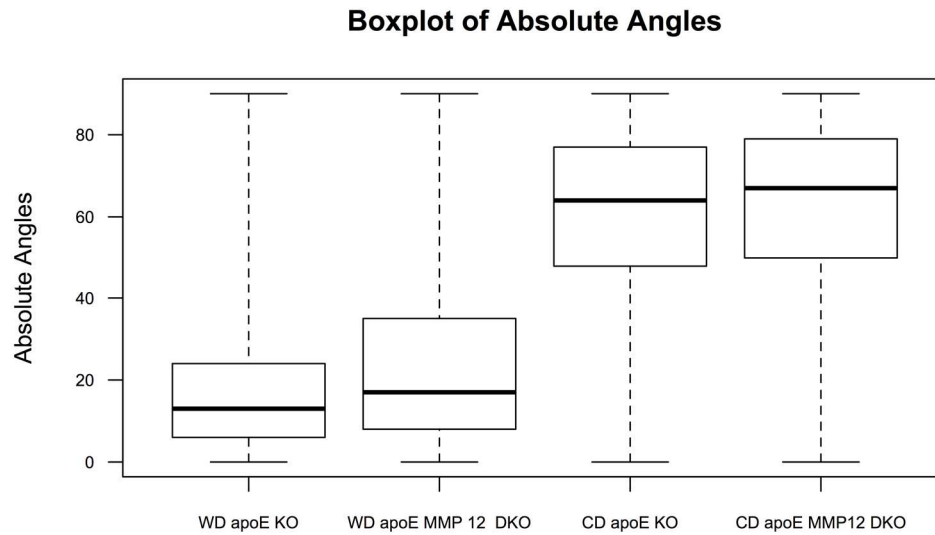
Figure 3.4. A boxplot of the four treatment groups showing the median, first, and third quartiles for each strain on a chow diet (CD) and Western diet (WD). apoE KO, apolipoprotein E knockout; apoE MMP12 DKO, apolipoprotein E matrix metalloproteinase-12 double knockout.

Table 3.1. Summary of mean effect and standard error for each independent variable. The coefficient of determination of the fitted model is $R^2 = 49.9\%$

| Factor | Estimate | 95% Confidence Interval | Standard Error | P-Value |
|---|---|---|---|---|
| Intercept, $C_0$ | 62.83 | | 2.03 | <0.05 |
| Diet (Western), $C_1$ | -43.35 | (-37.73, -48.96) | 2.86 | <0.05 |
| Location (Thoracic), $C_2$ | -0.84 | (-1.00, -0.67) | 0.09 | <0.05 |
| Depth (Adventitia), $C_4$ | 0.29 | (0.08, 0.50) | 0.11 | 0.027 |

CHAPTER 4

# DIET ALTERS AGE-RELATED REMODELING OF AORTIC EXTRACELLULAR MATRIX IN MICE SUSCEPTIBLE TO ATHEROSCLEROSIS

## 4.1 Abstract

Collagen is an important extracellular matrix protein providing overall strength to many biological tissues. A major challenge in understanding how collagen contributes to the functional properties of the arterial wall is identifying how vascular cells respond to mechanical loading by restructuring the surrounding extracellular matrix. Therefore, the objective of this study was to evaluate collagen architecture to understand the remodeling capabilities of the aorta during aging with or without atherosclerotic lesion development. We hypothesized that changes in collagen fiber orientation are initiated by endothelial dysfunction. Second-harmonic generation microscopy was used to visualize the three-dimensional organization of collagen throughout the aortic wall and to exam the structural differences in mice at 6 weeks and 6 months of age on a control chow diet and mice at ~7.5 months of age maintained on high-fat diet Western diet. Image analysis was performed on thoracic and abdominal sections of the aorta from each mouse to determine fiber orientation, with the circumferential direction (0°) and the blood flow direction (axial ±90°) as the two reference points. We found that average collagen fiber angle diverges with aging

in apoE KO mice on chow diet versus those on Western diet. Compared to 6-week old apoE KO mice, multiple regression analysis showed a significant difference in average absolute fiber angle in response to age and high-fat diet. On average, absolute fiber angle increased by 26.4° in older mice on the same diet and decreased 22.4° in mice fed a Western diet for 6 months. Our data indicate that the aortas of 6-week old apoE KO mice have an absolute collagen fiber angle in the inner media of 35.2±1.9° but that fibers become more circumferentially aligned to 12.5° after 6 months of Western diet feeding. In contrast, collagen fiber absolute angle undergoes a significant increase in apoE KO mice fed a chow diet for 6 months, with fibers in the inner media becoming more axially aligned, at 61.6°. Differences in collagen fiber orientation did not correlate with differences in total collagen content for the different treatment groups. We observed a significant increase in total collagen content as mice aged, independent of diet. To determine if these changes were a result of increased endothelial dysfunction, we compared immunohistochemical staining of two endothelial–derived factors, intercellular adhesion molecule-1 (ICAM-1) and endothelial nitric oxide synthase (eNOS), in older mice to 6-weeks old control mice. We found that eNOS decreases significantly with age, but ICAM-1 showed no significant differences with age or diet. Comparison of systemic blood pressures and time-averaged blood flow velocities in young and older mice on different diets indicated that the collagen fiber angle changes with age were not driven by altered hemodynamics. To date, the stimulus for vascular remodeling in this study remains inconclusive. However, we conclude that the aorta displays a

distinct remodeling response in the presence of atherogenic stimuli, even in non-lesioned areas, as observed by a shift in collagen fiber orientation.

## 4.2 Introduction

Atherosclerosis is a chronic inflammatory disease of the arterial wall, constituting a significant source of morbidity and mortality in the United States. It can be classed as a disease of aging (Wang & Bennett et. al., 2012) or a result of unhealthy diet, such that increasing age or low-density lipoprotein cholesterol can be independent risk factors for the development of atherosclerosis (Wang & Bennett et al., 2012). A major pathological change often preceding the development of atherosclerosis and associated with vascular aging is endothelial dysfunction, a diminished production/availability of nitric oxide and/or an imbalance between vasoconstricting and vasodilating substances produced by or acting on the endothelium (Hadi et. al, 2005; Park & Park, 2015).

During the last 3 decades, it has been shown that the vascular endothelium is an active organ regulating vascular tone and the maintenance of homeostasis (Hadi et. al, 2005). However, maintenance of vascular homeostasis as observed by changes in collagen fiber orientation associated with disease has not been attributed to mechanisms aside from mechanics or hemodynamics (Canham et al., 1996; Holzapfel, 2008; Holzapfel & Ogden, 2010; Badel et. al., 2012). Endothelial physiology has largely been overlooked as a factor promoting reorganization of collagen fibers to maintain homeostasis.

An important endothelial-associated and leukocyte-associated transmembrane protein important for stabilizing cell-cell interactions and facilitating leukocyte endothelial migration is intercellular adhesion molecule-1 (ICAM-1). ICAM-1 on the surface of vascular endothelial cells is closely related to the formation of early atherosclerotic lesions (Morisaki et al., 1997) and adhesion molecules are of central importance in the maintenance of tissue homeostasis (Yoneshige et al., 2015). A previous study conducted by Martinelli and colleagues suggests that ICAM-1 mediated endothelial nitric oxide synthase (eNOS) activation is important in basic immune function and provides a key link in the molecular network governing endothelial cell compliance to diapedesis (Martinelli et al., 2009).

Endothelial dysfunction associated with decreased nitric oxide stimulates adhesion molecules and causes acute inflammatory responses, proliferation of smooth muscle cells, and production of extracellular matrix, which all further contribute to cardiovascular disease (Pepine, 1998). We reasoned that collagen fiber realignment may be influenced by this process because of its involvement with surrounding extracellular matrix components. Furthermore, nitric oxide production is essential to maintenance of physiological contractile tone by arterial smooth muscle, and long-term changes in active contractile tone may be associated with compensatory alterations in passive mechanical behavior of the vessel. Therefore, we hypothesize that endothelial dysfunction is a stimulus for vascular remodeling and collagen fiber reorganization in the apolipoprotein E (apoE) knockout (KO) mouse.

61

Apolipoprotein E is an essential ligand for the uptake and clearance of atherogenic lipoproteins. Wild-type mice are resistant to the development of atherosclerosis. However, when mice with inactivated apoE genes are given diets that are normal, high in fat, or rich in cholesterol, the plasma cholesterol concentration in these mice significantly increases, which leads to rapid and severe atherosclerosis (Tian et al., 2015). The pathophysiology in apoE KO mice is similar to that in humans in regards to vascular distribution of lesions, cellular components, and overall lipid content of the lesions (Zhang et al., 1992). Thus, apoE KO mice are regarded as one of the best small animal models for studying the development of atherosclerosis (Fetterman et al., 2013; Weingärtner et al., 2015; Yi et al., 2010).

In a previous study, we reported the use of a SHG imaging technique to quantify collagen fiber distribution and alignment in the apoE KO mouse in lesion-free regions of the vessel wall. We employed a novel statistical analysis to study 3D fiber distribution and to provide details on differences in collagen fiber orientation in mice on chow diet versus Western diet (Watson, 2016). In this paper, we have used the methods published by (Watson et al., 2016) to report that diet alters age-related remodeling in the apoE knockout mouse model of atherosclerosis. We show that collagen fiber angular distribution diverges with aging in apoE KO mice on chow diet vs. those on Western diet, despite similar increases in total arterial collagen content. In addition, we demonstrate using in vivo physiological measurements that alterations in collagen fiber angle distribution are not driven by significant changes in aortic hemodynamics.

## 4.3 Materials and Methods

Three sets consisting of 5 apoE KO mice (Nakashima et al., 1994) each were placed into different treatment groups. All groups received chow diet (3.1 kcal per gram, composed of 24 kcal% protein, 58 kcal% carbohydrates, and 18 kcal% fat) for the first 6 weeks after weaning. The first group (2 females, 3 males) was euthanized after 6 weeks, whereas group 2 (3 females, 2 males) was maintained on a chow diet for an additional 4.5 months before euthanasia and group 3 was transferred to a high-fat Western diet (4.5 kcal per gram, 15 kcal% protein, 43 kcal% carbohydrates, and 42 kcal% fat) for an additional 6 months and euthanized at ~7.5 months of age. The Western diet was used to promote hypercholesterolemia and atherosclerotic lesion formation within the aorta of the mice in group 3 (no females, 5 males).

Sample Preparation

All mice were handled in compliance with protocols approved by the University of South Carolina Institutional Animal Care and Use Committee. Following the duration of each diet, mice were ethically euthanized at 6 weeks old or ~7.5 months old by carbon dioxide asphyxiation. Mice were then perfused through the left ventricle with heparinized normal saline for five minutes at physiological pressure, followed by pressure perfusion fixation for 10 minutes with 10% neutral buffered formalin. Thoracic and abdominal aortas were harvested from apoE KO mice from each age group and diet. Under a dissecting microscope, each aorta was opened longitudinally for *en face* examination.

63

Segments from non-lesioned areas of the thoracic and abdominal aorta were sampled at the level of the fourth intercostal arteries and the infrarenal abdominal aorta, respectively. The aortic segments were flattened to a slide and labeled according to the direction of blood flow for each specimen.

Second-harmonic generation microscopy

To image collagen fibers, we used a custom-built hybrid two-photon excitation fluorescence (TPEF) second harmonic generation microscope (SHG) (Liu et al., 2011). Optical sectioning with SHG microscopy permits visualization of collagen fibers throughout the vessel wall thickness without staining. The SHG signals were collected from the forward direction through an Olympus 1.4 NA oil immersion condenser (Liu et al., 2011, Liu et. al., 2013). The XYZ stage of the microscope was controlled through three orthogonally mounted motors to collect image stacks throughout the vessel wall thickness using a 60X objective. The area in pixels for each image was 512x512 pixels with the actual calibrated image being 176x176 microns.

Semi-Automated Image Analysis

Using Continuity software 6.4b, a previously described analytic protocol for automatic angle recognition (Wicker et al., 2008; Tang et al., 2014) was used to quantify collagen fiber orientation. The software determined collagen fiber orientation using the circumferential (0°) and axial directions (±90°) as the reference points. The individual, local fiber orientations were determined in the z-

64

θ plane. Each image of the stack was analyzed and provided fiber angle measurements to be used in a multivariate statistical analysis.

Multiple Regression Analysis

For this study, we used a statistical method previously described in (Watson et al., 2016) that consisted of two mixed models implemented in the R package "lme4" (Bates et al., 2014). Mice in group 2 and group 3 were not exactly age-matched; therefore, two models were used so that age/diet was a combined variable that was different in group 2 vs group 3. Independent variables were mouse age/diet, anatomical location, and radial position ('depth'). The absolute angle can be calculated from the formula: $\beta = \beta_0 + \beta_1 \text{(age/diet)} + \beta_2 \text{(depth)} + \beta_3 \text{(location)}$, where $\beta$ is the mean fiber angle for a given set of conditions, $\beta_0$ is the global mean fiber angle for the 6-week old mice in the inner media of the abdominal aorta, and $\beta_i$ are coefficients describing the contribution of each significant independent variable. To account for the three layers of the artery, we investigated depth (radial position) as a categorical variable. An observation from depth in the first third of the stack ($0 < t < 1/3$, where $t$ is the wall thickness) relates to collagen fibers in the inner media, an observation from the middle third ($1/3 < t < 2/3$) corresponds roughly to collagen fibers in the outer media, and an observation from the final third ($2/3 < t < 1$) is equivalent to fibers in the adventitia. Variables with $p < 0.05$ in the final model were considered to be statistically significant contributors to the mean average fiber angle.

Tissue Preparation for Histology

Fixed segments from the third intercostal space of mouse aortas dissected at the time of tissue harvest were embedded in 10% agarose gel for ease of handling and to obtain appropriate vertical orientation of the small specimens. Agarose blocks were dehydrated in graded alcohols and processed using conventional methods before paraffin embedding. Following embedding, the aortic segments were sectioned transversely at 5µm to produce ring-shaped cross-sections.

Collagen Content by Picrosirius Red (PSR) Staining

Cross-sections of aortic tissues were deparaffinized and rehydrated in descending grades of alcohol before incubation with Direct Red (0.1% in saturated picric acid, Sigma Aldrich, St. Louis, MA) for 90 minutes. The slides were washed in 0.01 N HCl and then dehydrated in ascending grades of alcohol and xylene before mounting with Permount. PSR-stained tissue sections were analyzed by cross-polarized transmitted light microscopy on a Zeiss Axioskop 2 (Carl Zeiss Microscopy, Thornwood, NY). PSR-stained sections were imaged in brightfield for total area measurements and under cross-polarized transmitted light for collagen area measurement. Cross-polarized transmitted light images were segmented in ImagePro Plus software (Media Cybernetics, Silver Springs, MD) to measure the area of collagen birefringence in each aortic section. Fractional area of collagen was calculated as area of collagen birefringence (pixels)/ total area of aortic wall (pixels) x 100%.

Collagen Type I Detection by Immunohistochemistry

For immunohistochemical detection of Type I collagen, we followed a standard protocol involving deparaffinization of the tissue, antigen retrieval with 10mM citrate buffer, blocking with 10% donkey serum, staining with primary antibody against collagen type I (1:20 dilution, anti-collagen type 1 rabbit polyclonal, Calbiochem, San Diego, CA), and visualization with a fluorescently-labeled secondary antibody (1:50 dilution, Rhodamine Red X donkey anti-rabbit IgG, Jackson ImmunoResearch, Westgrove, PA). Nuclei were counterstained with Hoechst 33258 (1:10,000 dilution, Sigma Aldrich, St. Louis, MO). Our epifluorescence microscope (Zeiss Axioskop 2) was equipped with a standard filter set to detect FITC (ex. 450-490 nm; em. 500-550nm) and Rhodamine (ex. 538-562nm; em. 570-640nm). A CCD camera (Axiocam, Zeiss) with appropriate acquisition software (Axiovision) captured 8-bit images using the 5x objective. The merged green (FITC channel) and red (Rhodamine channel) images provided the total vessel wall area, while the Rhodamine image provided the collagen area. Control sections were not stained with primary antibody and provided the baseline threshold to eliminate nonspecific background fluorescence. Epifluorescent images were segmented in ImagePro Plus software to measure the area of collagen I-specific staining in each aortic section. Fractional area of collagen I was calculated as area of collagen I staining (pixels)/ total area of aortic wall (pixels) x 100%.

Immunohistochemistry for ICAM-1

Intercellular adhesion molecule-1 (ICAM-1) was used as a marker of endothelial dysfunction in the aortic specimens. Adhesion molecule expression was evaluated by staining fixed cross-sections of aortic specimens with a primary monoclonal antibody (mAb) to ICAM-1 (1:50 dilution, KAT-1 clone, eBioscience, San Diego, CA) after deparaffinzation and blocking of the endogenous peroxidases with 3% hydrogen peroxide. A biotinylated donkey anti-rat secondary antibody (1:100 dilution, Jackson ImmunoResearch, Westgrove, PA) was used to detect the primary antibody and was visualized using HRP-conjugated streptavidin (1:250 dilution, Jackson ImmunoResearch, Westgrove, PA). Diaminobenzidine (DAB, Vector Laboratories) was used as the chromogen with a color development time set at 7 minutes. Nuclei were stained with Gill's hematoxylin and sections were dehydrated in ascending grades of alcohol and xylene before mounting with Permount.

Immunohistochemistry for eNOS Expression

Endothelial nitric oxide synthase (eNOS) was used as a second marker of endothelial dysfunction in the aortic specimens. eNOS expression was evaluated by staining fixed aortic sections with a primary polyclonal antibody (pAb) (1:100 dilution, Novus Biologicals, Littleton, CO) after deparaffinzation and blocking of the endogenous peroxidases with 3% hydrogen peroxide. A biotinylated donkey anti-rabbit secondary antibody (1:100 dilution, Jackson ImmunoResearch, Westgrove, PA) was used to detect the primary antibody and was visualized

using HRP-conjugated streptavidin (1:250 dilution, Jackson ImmunoResearch, Westgrove, PA). DAB (Vector Laboratories) was used as the chromogen with a color development time set at 4 minutes to avoid overstaining. Nuclei were stained with Gill's hematoxylin and sections were dehydrated in ascending grades of alcohol and xylene before mounting with Permount.

*In vivo* Physiological Measurements

Tail-cuff plethysmography

Prior to blood pressure measurements, all mouse body weights (in grams) were recorded. Mouse blood pressure was monitored by a tail-cuff blood pressure analysis system (MC4000; Hatteras Instruments, Cary, NC). Systolic and diastolic blood pressures were recorded over 5 preliminary equilibration cycles and 10 measurement cycles. Mice were acclimated to the plethysmography system for three days minimum preliminary to final blood pressure recording.

Ultrasonography

Mice were anesthetized with 1.5-2.5% isoflurane in oxygen prior to and throughout ultrasound measurements on a Vevo 770 small animal ultrasound machine (VisualSonics, Toronto, CN). To acquire pulse wave and aortic diameter measurements in the thoracic aorta, mice were placed in a laterally recumbent position. For measurements in the abdominal aorta, mice were placed in a supine position. Ultrasound measurements correspond with the anatomical

locations of collagen fiber measurements at the level of the fourth intercostal space and the abdominal aorta. B-mode images, peak wave velocity measurements, and M-mode images were obtained using the RMV-707 probe (VisualSonics) with a broadband frequency up to 45 MHz. M-mode images were used to measure vessel diameter during systole and diastole.

### 4.4 Results

Statistical Analysis

We report the estimates of model parameters, standard errors and p-values of the two separate models in Tables 1 and 2. In Model 1, the grand mean estimate of collagen fiber angle in the inner media of the aorta of 6-week old mice ($\beta_0$) is 35.17° (Table 4.1). We conclude that the mean absolute collagen fiber angle in the inner media of the mice fed a chow diet for 6 months (Group 2) is 26.4±2.7 degrees larger than that of the 6-week old mice, or 61.6°. Average fiber angle increases progressively with radial position in these mice, by 1.1° for the range $1/3 < t < 2/3$ (outer media) and by 3.8° for the range $2/3 < t < 1$ (adventitia). No significant dependence of fiber angle on aortic location (thoracic vs. abdominal) was observed in Model 1.

In Model 2, the grand mean estimate of collagen fiber angle in the media of the abdominal aorta of 6-week old mice ($\beta_0$) is 34.9°±1.9° (Table 4.2). Given the standard errors in the means, this value is not significantly different from the value obtained using Model 1. We conclude that the mean absolute collagen fiber angle in the medial layer of the abdominal aorta of the 6 months Western

diet fed mice is about 22° smaller than that of the 6-week-old mice on a chow-diet, or 12.5°. We have only reported values that are significant at p<0.05.

Figure 4.1 shows a boxplot comparing the median, first, and third quartiles of collagen fiber angle observations for the apoE mouse strain at different ages on chow diet and on Western diet after 6 months.

Constructed 3D Histograms of Collagen Fiber Distribution Across Aortic Wall

Figure 4.2 provides an illustration of representative 3D histograms of collagen fiber angle distribution for apoE KO mice on chow diet at 6 weeks old and 6 months old and on Western diet at ~7.5 months old. Zero degrees is the circumferential direction. Figure 4.2 presents the distribution of collagen fiber angles in thoracic aorta specimens, and the corresponding fiber angle distribution in abdominal aorta specimens is very similar (data not shown). The 3-D histograms reflect image stacks for one individual mouse on each diet.

IHC Analyses

Fractional collagen content (% area) for each of the three treatment groups obtained by Picrosirius Red staining (Figure 4.3) showed that collagen content increases significantly with age from 6 weeks to 7.5 months (P<0.05). Qualitatively similar results were obtained from the collagen type I immunohistochemistry (IHC) analysis (Figure 4.4). As age increases, aortic collagen type I content increases significantly; however, there are no statistical differences between mice of nearly the same age on different diets. The

fractional collagen content measured by IHC is greater than that measured by PSR because PSR only shows mature, well organized collagen that gives rise to birefringence. IHC shows all collagen type I, even immature or disorganized collagen, as long as the relevant epitopes are present.

Analysis of endothelial markers revealed ICAM-1 expression increases slightly with age, although these results are not significantly different with age or diet (Figure 4.5). Most importantly, we observed a significant decrease in eNOS expression as mice aged. However, there was no a statistical difference in eNOS expression between mice of nearly the same age on different diets (Figure 4.6).

Physiological Measurements

Six-month-old mice on Western diet demonstrate increased gain in body weight compared to 6-month-old mice on chow diet ($31.05 \pm 4.21$g vs $24.53 \pm 2.99$g $p < 0.05$), which further supports differences in these mice independent of aging. Body weight for 6-week-old mice was $16.45 \pm 2.55$g (Figure 4.7). However, despite the increase in body weight, systolic and diastolic aortic diameters were not significantly different between mice on chow diet for 6 months vs. those on Western diet (Figure 4.8).

As shown in Figures 4.9 and 4.10, there were no significant differences in blood pressures or blood flow rates between the different treatment groups.

72

## 4.5 Discussion

Factors that can influence geometrical vascular remodeling include changes in blood flow velocity, blood pressure, and/or vascular injury. Changes in collagen fiber rearrangement represent a more subtle form of vascular remodeling . Collagen fibers have preferred directions associated with the mechanical stresses on the tissue (Holzapfel, 2001). Understanding the microscopic structure of collagen fibers and changes in their arrangement can provide information on how arteries remodel to maintain homeostasis. Quantitative analysis of collagen fiber angles from the atherosclerotic specimens used in our studies has been informative in defining the distribution of collagen and the factors that contribute to the remodeling capabilities of the aorta.

Our research has shown that as apoE KO mice age, there is a relative redistribution of collagen fibers to become more longitudinally oriented, increasing the average fiber angle by 26.4°. The inclusion of a Western diet with aging resulted in a different rearrangement of collagen fibers which causes an overall decrease in angular distribution by 22.4°. With regard to the mean fiber angle, the structure-based constitutive model used by Collins et al. (2011) predicted angle for normal (wild type) mouse infrarenal abdominal aorta is 39° with respect to the Z-direction (51° relative to the θ-direction). Our observed mean fiber angle for the infrarenal abdominal aortic media is ~36° in 6-week-old chow diet-fed mice, slightly lower than the predicted value. However, our result represents the experimental average of a 3-dimensional distribution of fibers as opposed to a parameter identified by fitting a four fiber-family model to biaxial

73

test results.  In addition, our mice were younger than the 2-3 month old mice used by Collins et. al. (2011).

We show that there are no significant differences between the average absolute angles based on anatomical location (thoracic versus abdominal) in aging mice on the chow diet. However, small but significant differences were observed in aging mice that are transferred to a Western diet, with an increase in average fiber angle of 4.6±0.1° in the thoracic aorta vs. the abdominal aorta. Our data suggests that diet and age were the most significant factors causing alteration of the mean collagen fiber angle.

In trying to understand the cause of shifts in collagen fiber arrangement, we have assessed physiological factors such as blood pressure (BP) and blood flow rate. Our blood pressure results reveal no significant differences among age or diet groups. These results are consistent with several studies evaluating BP that have shown that BP levels in young-adult (up to 7.5 months) hypercholesterolemic apoE KO mice fed a standard chow diet or a Western-type diet are similar to those of control mice, in our case the 6-week-old mice (d'Uscio et al., 2002; Barton et al., 1998; Wassman et al., 2004; Gervais et al., 2003; Arruda et al., 2005; Noguieira et al., 2007). Our blood flow rate measurements were similar to those acquired *in vivo* in the abdominal aorta of apoE KO mice using phase-contrast magnetic resonance imaging. Amirbekian et al. (2009) recorded a mean blood flow rate in the apoE KO mouse infrafrenal abdominal area of 2.95±1.62 ml/min and a mean aortic diameter for the same area of 0.69±0.04 mm. Our 6-week-old mice had a mean blood flow rate of 2.95±2.65

ml/min; however, we measured a larger abdominal aortic diameter at 0.96±0.5 mm. These young mice did not show an aortic diameter or mean blood flow rate significantly different than older mice of the same strain on chow or Western diet.

Beyond hemodynamics, we also investigated total collagen content and changes in endothelial dysfunction by measuring two endothelial-derived factors, ICAM-1 (Figure 4.3) and eNOS expression (Figure 4.5). Our data reveal that mature, birefringent collagen content as well as collagen type 1 increase significantly with aging. Collagen content also significantly differed between chow vs. Western diet mice. It was expected that ICAM-1 would increase with aging and Western diet because of increased lesion formation (Nakashima et al., 1998);however, no significant differences were detected. More interestingly, in our study eNOS, an established contributor to endothelial dysfunction in the apoE KO mouse (Vasques et al, 2012), was significantly different in young vs. older mice but not in mice on 6 months chow diet vs. 6 months Western diet. A previous study that reviewed how endothelial dysfunction in the apoE KO mouse is influenced by aging, gender, and diet revealed that impaired endothelial nitric oxide-dependent relaxation response to acetylcholine, associated with plaque formation (Bonthu et al, 1997; Johansson et al., 2005, and Crauwel, et al.; 2005), is aggravated by Western-type diet (Deckert et al., 1999; d'Uscio et al., 2001; Jiang et al., 2001) and by aging (Crauwel et al., 2003; Guns et al., 2008). While we detected a decrease in eNOS with aging, we did not find significant changes due to Western diet. However, a limitation of this study is that chow diet fed mice were mixed genders and Western diet fed mice were all male. This gender

75

distribution may have influenced our hemodynamic and eNOS studies, as estrogen results in upregulation of eNOS and initiates signaling pathways that enhance cardioprotection (Murphy & Steenbergen, 2007). In addition, there is a limitation of the small sample size used for this study, which did not allow us to isolate gender effects in the older mice in Group 2. Based on our statistical analysis, we suggest that two different mechanisms may be underlying changes in collagen fiber reorganization within our mouse study in respect to aging on Western diet vs. aging on chow diet.

## 4.6 Conclusion

Our data indicate that the aortas of 6-week-old apoE KO mice have a significantly lower mean collagen fiber angle when compared to older mice (6 months to ~7.5 months old) on chow diet, but a significantly greater mean fiber angle compared to 7.5 month old mice on a Western diet. We demonstrate that collagen fiber reorientation can occur either in the circumferential direction or the axial direction. These differences show that diet alters age-related remodeling and suggests that changes in the ECM may result from atherogenic stimuli.

In this study, we have not detected significant hemodynamic changes (blood pressure, volumetric flow rates) or structural changes (aortic diameter) in either the thoracic or abdominal regions which were sampled for collagen fiber angle measurements. Furthermore, we have sampled in areas without lesions, ruling out pathological wall remodeling specific to plaque development. We have also demonstrated that, starting with an average fiber angle of 35° in young adult

mice, collagen fiber reorientation with aging can result either in more longitudinally oriented fibers or in more circumferentially oriented fibers, depending on diet.  While Western diet feeding is known to have many biochemical and physiological consequences in apoE KO mice (Moghadasian et. al., 1999; Plump et. al., 2005), we have focused here on its role in promoting endothelial dysfunction.

A theoretical study conducted by Morin and colleagues (Morin, et al., 2015) suggests that, in the absence of geometric remodeling, collagen fiber orientation may be altered as the result of a change in fiber mechanical properties relative to the properties of the surrounding tissue/matrix. Therefore, potentially productive avenues for future work would include measuring properties of the individual collagen fibers with age and diet, as well as investigating alterations in active mechanical response related to decreased nitric oxide signaling.

**Table 4.1:** Parameter estimates of the multiple regression model for 6 months chow diet fed apoE KO mice vs 6 weeks chow diet fed mice of the same strain.

| Variable | Coefficient | Estimate, degrees | Standard Error | p-value |
|---|---|---|---|---|
| Global Mean | $\beta_0$ | 35.2 | 1.9 | <0.05 |
| 6 Months Chow diet | $\beta_1$ | +26.4 | 2.7 | <0.05 |
| Outer medial Layer (1/3 < t < 2/3) | $\beta_2$ | +1.1 | 0.1 | <0.05 |
| Adventitial Layer (2/3 < t < 1) | $\beta_3$ | +3.8 | 0.1 | <0.05 |

**Table 4.2:** Parameter estimates of the multiple regression model for 6 months Western diet fed apoE KO mice vs. 6 weeks chow diet fed mice of the same strain.

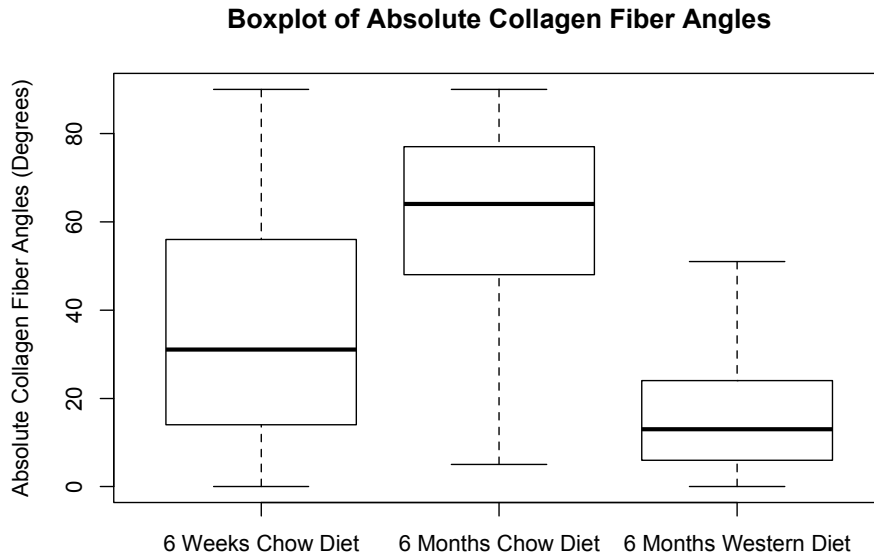| Variable | Coefficient | Estimate, degrees | Standard Error | p-value |
|---|---|---|---|---|
| Global Mean | $\beta_0$ | 34.9 | 1.9 | <0.05 |
| 6 Months Western diet | $\beta_1$ | -22.4 | 2.7 | <0.05 |
| Adventitial Layer (2/3 < t < 1) | $\beta_2$ | -0.5 | 0.2 | <0.05 |
| Thoracic Aorta | $\beta_3$ | +4.6 | 0.1 | <0.05 |

**Boxplot of Absolute Collagen Fiber Angles**



Figure 4.1: Average collagen fiber angle diverges with aging in apoE KO mice on chow diet vs. those on Western diet. Compared to 6-week old apoE KO mice, multivariate analysis showed a significant difference in average absolute fiber angle in response to age and high-fat diet. On average, absolute fiber angle was increased by 26.4° in older mice on chow diet and reduced by 22.4° in mice fed a Western diet for 6 months.

**Collagen Fiber Angle Distribution in Thoracic Aorta of apoE KO Mouse on a Chow Diet for 6 Weeks**
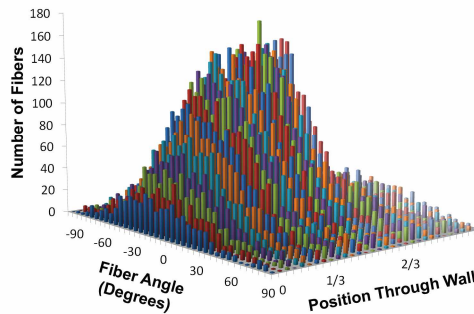


**Collagen Fiber Angle Distribution in Thoracic Aorta of apoE KO Mouse on a Chow Diet for 6 Months**
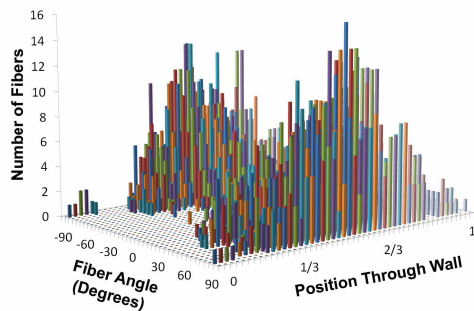


**Collagen Fiber Angle Distribution in Thoracic Aorta of apoE KO Mouse on a Western Diet for 6 Months**

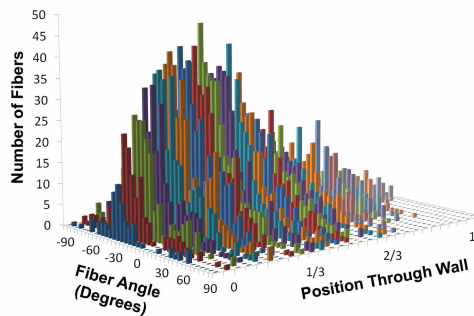Figure 4.2: Three-dimensional histograms showing distribution of collagen fiber angles in a) apoE KO mice fed a chow diet for 6 weeks (6 weeks old), b) apoE KO mice fed a chow diet for 6 months (~7.5 months old), c) apoE KO mice fed a Western diet for 6 months (~7.5 months old). Radial wall position (tissue depth) is designated as zero at the luminal surface and as one at the outer edge of the adventitia.

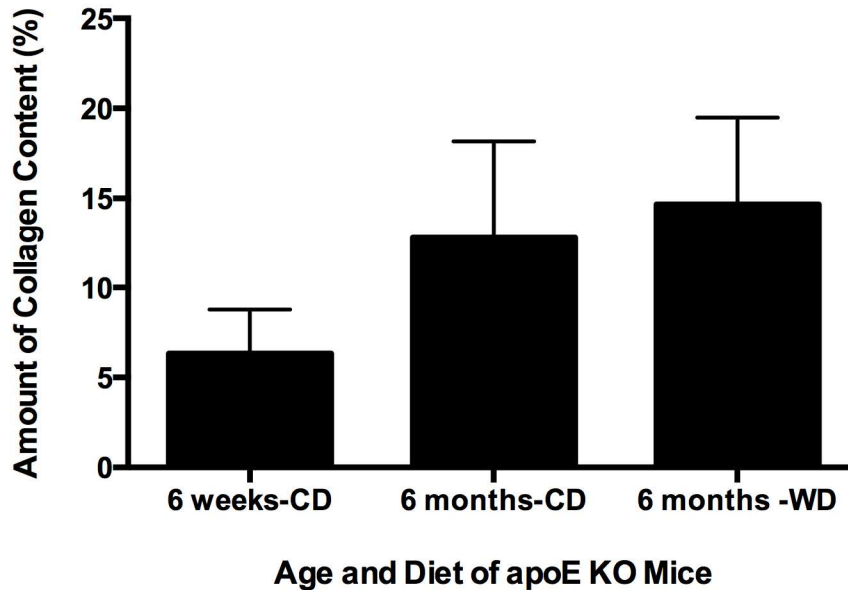**Aortic Collagen Content in apoE KO mice on Chow Diet or Western Diet at 6 Weeks or 6 Months of Age**

Figure 4.3: Fractional collagen content (% area) for each of the three treatment groups obtained by Picrosirius Red staining. Collagen content increases significantly with age from 6 weeks to 7.5 months (P<0.05), but is not altered by Western diet. CD = chow diet; WD = Western diet

**Aortic Collagen Type 1 Content in apoE KO mice on Chow Diet or Western Diet at 6 Weeks or 6 Months of Age**

Figure 4.4: Collagen type 1 (% area) for each of the three treatment groups obtained from immmunohistochemistry. Collagen type 1 increases significantly with age from 6 weeks to 7.5 months (P<0.05), but is not altered by Western diet. The % collagen is greater by IHC as opposed to PSR because PSR only shows mature, well organized collagen with birefringence. IHC shows all collagen type I, even immature.

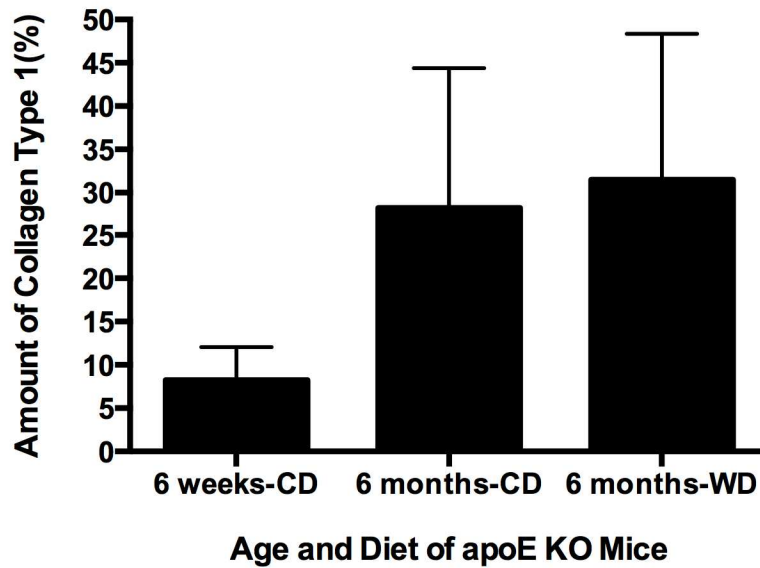# Aortic ICAM-1 Expression in apoE KO mice on Chow Diet or Western Diet at 6 Weeks or 6 Months of Age
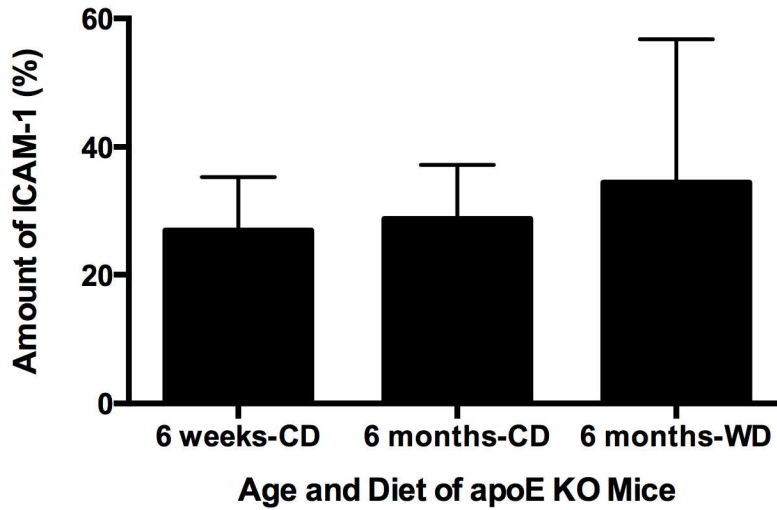


Figure 4.5: ICAM-1 expression (% area) for each of the three treatment groups obtained from immmunohistochemistry. Collagen type 1 increases with age from 6 weeks to 7.5 months, however, there is no significant differences.

**Aortic eNOS Expression in apoE KO mice on Chow Diet or Western Diet at 6 Weeks or 6 Months of Age**
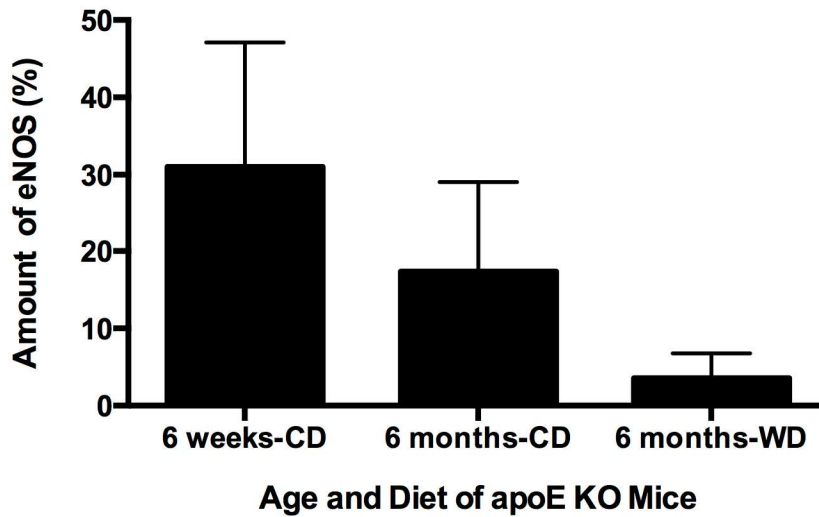
Figure 4.6: eNOS expression (% area) for each of the three treatment groups (n=5) obtained from immmunohistochemistry. *P<0.05

**Increasing Body Weight in apoE KO Mice**
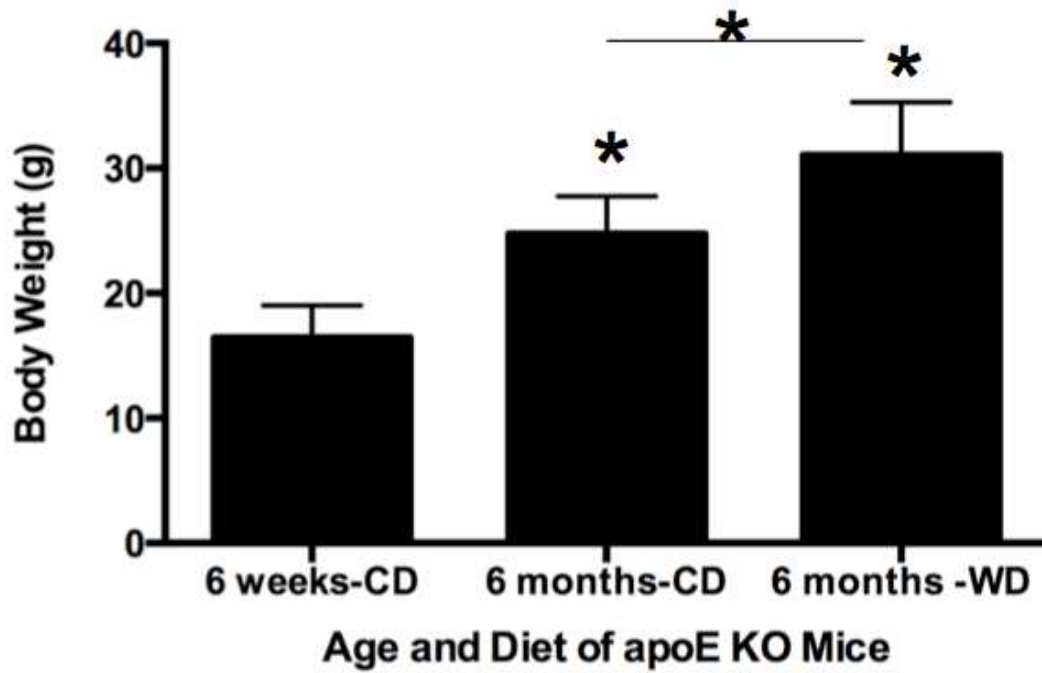
Figure 4.7: apoE KO mice (n=5) demonstrate significantly increased body weight in response to aging and diet. CD=chow diet; WD=Western diet; *$P<0.05$ vs. 6-week old mice; #$P<0.05$ vs. chow diet.

**Assessment of Aortic Diameters at Systole and Diastole Obtained from Ultrasound**

Legend:
- Thoracic Diameter at Systole
- Thoracic Diameter at Diastole
- Abdominal Diameter at Systole
- Abdominal Diameter at Diastole

Y-axis: Aortic Diameter (mm)
X-axis: Age and Diet of apoE KO Mice (6 weeks-CD, 6 months-CD, 6 months -WD)
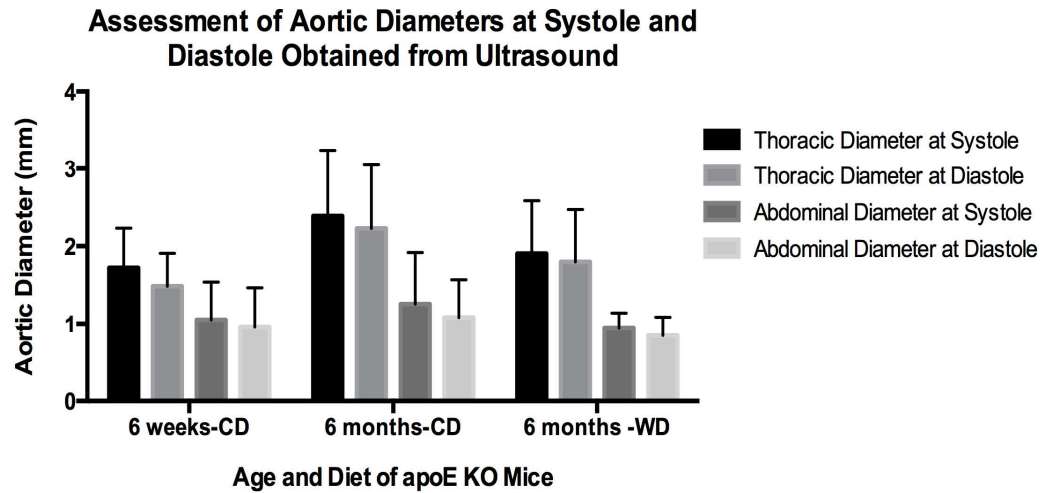
Figure 4.8: Systolic and diastolic aortic diameters obtained from ultrasound imaging for the three treatment groups (n=5 per group).

**Average Blood Pressure for apoE KO Mice on Chow Diet or Western Diet at 6 Weeks or 6 Months of Age**
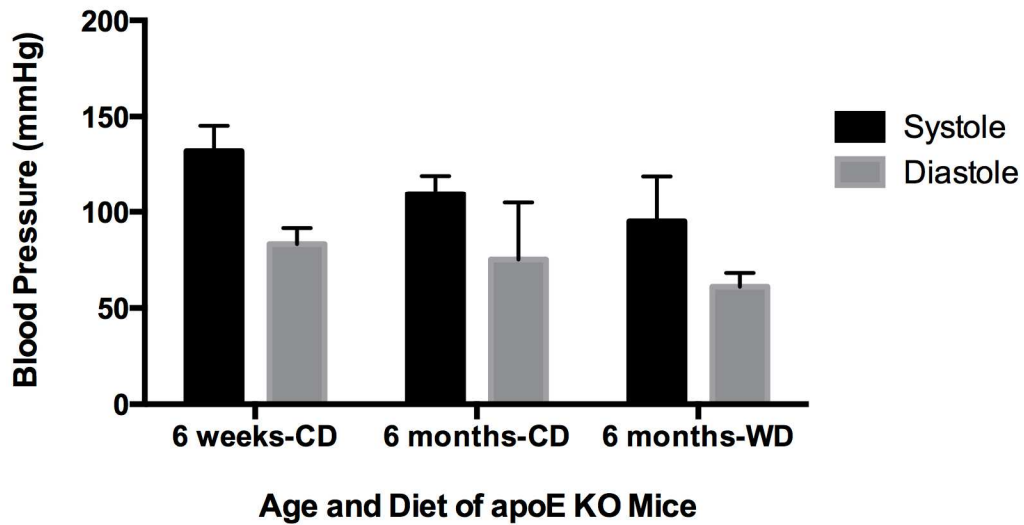
Figure 4.9: Systolic and diastolic blood pressure measurements from apoE KO mice for the three treatment groups (n=5 per group).

**Mean Volumetric Blood Flow for apoE KO Mice on Chow Diet or Western Diet at 6 Weeks or 6 Months of Age**
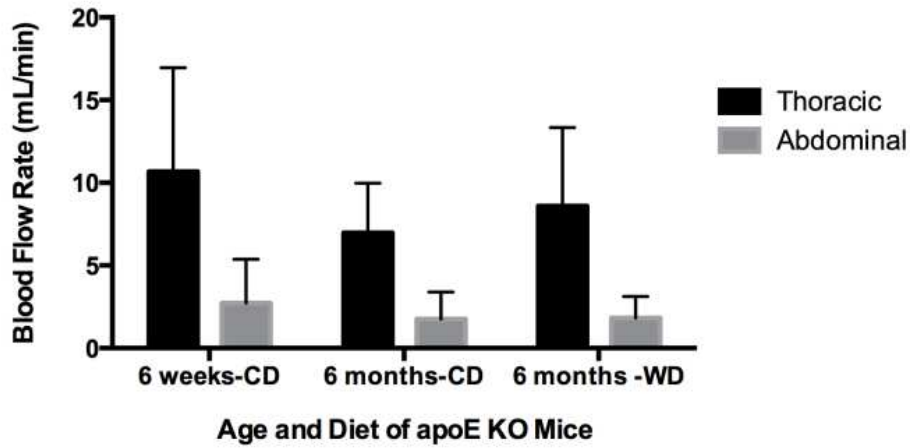
Figure 4.10: Mean volumetric blood flow rate acquired from Doppler ultrasonography of thoracic and abdominal aorta at 6 weeks or after 6 months on diet for the three treatment groups.

## CHAPTER 5

## CONCLUSION

### 5.1 Summary and Future Directions

The distribution of collagen fibers plays a central role in the mechanical behavior of arterial walls. Changes in collagen fiber orientation reflect alterations in the extracellular matrix. Understanding factors that alter collagen fiber orientation therefore produces insight into the remodeling capabilities of the vessel, which is important in the study of atherosclerosis.

Among engineers and microscopists, one of the most popular emerging techniques for visualizing collagen fibers is SHG imaging, yet there have been few quantitative analyses of the data from experimental measurements. We exported the angle measurements into bivariate histograms and then designed a statistical method to compare these histograms. Oftentimes mean collagen fiber angle is predicted from biaxial mechanical test data using an assumed constitutive model to describe the material response of vascular tissue. Few experimental methods exist to acquire collagen fiber angle data through the vessel wall thickness. In addition, it is challenging to compare histograms that are bivariate. Therefore, we developed a method to compare distributions of absolute angles between different groups, controlling for diet, mouse strain, anatomical location, and depth (radial position) within the arterial wall. Data was extracted from bivariate histograms and analyzed in R, a programming language

www.manaraa.com

and statistical software. The multiple regression model that was designed and used allowed for quantification of changes in the aorta of two strains of mice (apoE KO and apoE MMP12 DKO). We were able to quantify layer-specific distribution of collagen fibers in a mouse model of atherosclerosis and to provide a quantitative analysis describing the observed changes. This study demonstrated a lot of variability as seen in the boxplots (Figure 4.1); however, we have convincing evidence suggesting that the variation in fiber distributions is related to diet and aging.

In Chapter 3, we measured over 20,000 angles from non-lesioned portions of the aorta at the fourth intercostal space and the infrarenal abdominal areas. The results of our analysis show a single fiber family. The 3D histograms of the chow diet-fed mice appear to reflect a bimodal distribution. We do not believe this represents two fiber families, but instead shows that the fibers are oriented with the blood flow direction, nearly +90 and -90 degrees.  The same trend was seen in apoE MMP9 DKO mice on both chow and Western diet.

Currently, we cannot correlate the shifts in collagen with a loss of elastin. Although increased collagen content in the aorta may be compensating for the loss of elastin (as observed in aortic aneurysm development), we have not measured elastin content. Furthermore, our blood pressure and ultrasound data does not suggest that there are significant hemodynamic changes within these aortas (Figure 4.9; Figure 4.10). Although fractional collagen content increased significantly between young adult mice and older mice, we observed no change in collagen deposition between chow diet fed and Western diet fed older mice.

Wall thickness measurements obtained during circumferential stress/hoop stress calculations (data not shown) show no statistical differences. We conclude that the changes observed in collagen fiber angle distribution in younger vs. older mice on Western diet may be a result of atherogenic stimuli. We have not been able to thoroughly dissect the mechanism underlying these changes but believe that using a larger sample size and a model without prior endothelial dysfunction (for comparison) should be part of future directions.

Future Directions
Bridging Fibers

We obtained images that illustrate alterations of the collagen fibers in aortic layers in the z-θ plane but provide no information about radially-oriented ("bridging") fibers. Vascular remodeling at the microstructural level in response to aging and/or diet could conceivably alter the number and distribution of bridging fibers in the r-θ plane.  A future goal of this study will be to observe and evaluate fiber organization in different planes to determine how these fibers are linked together to form a stable matrix.

Matrix Metalloproteinase-9

Previous studies have shown that the activity of matrix metalloproteinase-9 (MMP9) has an influence on compensatory vascular remodeling during atherosclerotic lesion growth and plays a key role in collagen remodeling (Lessner, et al., 2004; Frostegard, 2013). Preliminary data gathered in our lab

suggests that apoE MMP9 DKO mice fail to show a shift in collagen fiber distribution on chow versus Western diet (Figure 5.1). The apoE KO mice are susceptible to atherosclerosis due to a genetic defect in their ability to clear circulating plasma lipoproteins. In addition, lacking an MMP9 gene causes a deficiency in the ability to degrade structural protein(s) and potentially to remodel extracellular matrix in the vessel wall.

A future goal to understand our preliminary data would be an attempt to rescue vascular remodeling in the apoE MMP9 DKO mouse model using bone marrow transplantation (BMT). The artery can maintain vessel integrity if vascular remodeling occurs. The artery compensates for atherosclerotic lesion growth by remodeling to preserve lumen area. We will attempt to rescue remodeling in the apoE MMP9 DKO strain to demonstrate that leukocyte-derived MMP9 is essential for aortic remodeling in response to atherosclerosis. The apoE KO mouse will be used as the donor strain to obtain bone marrow cells. These cells will be intravenously injected into the recipient mouse, apoE MMP9 DKO. A previously published method will be used (Lessner, et al., 2002; Duran-Struuck & Dysko, 2009). Mice will be maintained on Western diet for 6 mos after BMT, followed by aorta harvest and collagen fiber analysis as in Specific Aim 1. BMTs can be used to demonstrate functional dependence on leukocyte-derived proteins in vivo and thus are preferred over *in vitro* methods, which do not always mimic the systems correctly (Duran-Struuck & Dysko, 2009). A potential difficulty is that MMP9 production by other cell types, such as smooth muscle cells, may also be required for remodeling and this will not be rescued by BMT.

**Collagen Fiber Angle Distribution of Chow Diet apoE MMP9 DKO Mouse Thoracic Aorta**

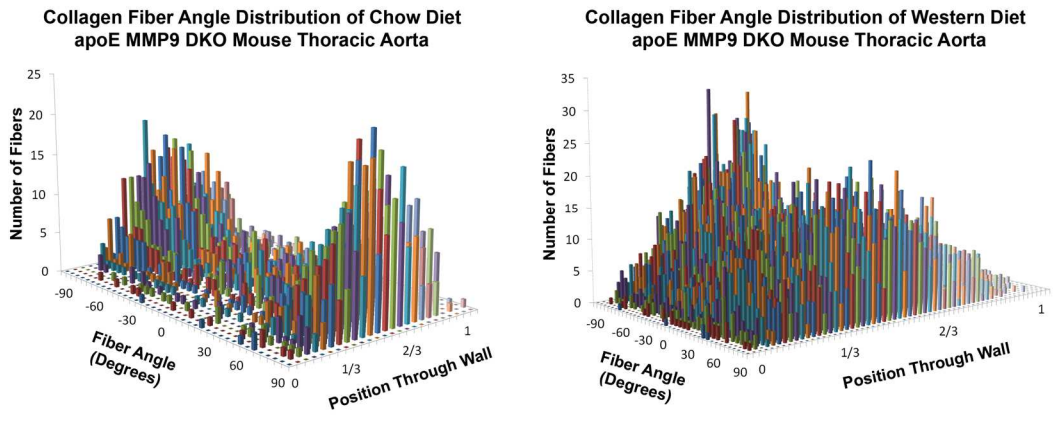**Collagen Fiber Angle Distribution of Western Diet apoE MMP9 DKO Mouse Thoracic Aorta**

Figure 5.1: 3-D histograms of representative fiber angle distribution as a function of relative distance from the lumen in the thoracic aorta of apoE MMP9 DKO mice on chow diet and on Western diet.

# REFERENCES

ABELA, G. S. Cholesterol crystals piercing the arterial plaque and intima trigger local and systemic inflammation. *Journal of clinical lipidology* **4**, 156–64.

ADIGUZEL, E., AHMAD, P. J., FRANCO, C. & BENDECK, M. P. (2009). Collagens in the progression and complications of atherosclerosis. *Vascular medicine (London, England)* **14**, 73–89.

ALEXANDER, J. J. (2004). The pathobiology of aortic aneurysms. *The Journal of surgical research* **117**, 163–75.

AMERICAN CANCER SOCIETY (2006). *Cancer Facts and Figures*. Atlanta.

ANDERSON, G. F. & CHU, E. (2007). Expanding priorities--confronting chronic disease in countries with low income. *The New England journal of medicine* **356**, 209–11.

ARIFLER, D., PAVLOVA, I., GILLENWATER, A. & RICHARDS-KORTUM, R. (2007). Light scattering from collagen fiber networks: micro-optical properties of normal and neoplastic stroma. *Biophysical journal* **92**, 3260–74.

ARRUDA, R. M. P., PEOTTA, V. A., MEYRELLES, S. S. & VASQUEZ, E. C. (2005). Evaluation of vascular function in apolipoprotein E knockout mice with angiotensin-dependent renovascular hypertension. *Hypertension* **46**, 932–6.

BADEL, P., AVRIL, S., LESSNER, S. & SUTTON, M. (2012). Mechanical identification of layer-specific properties of mouse carotid arteries using 3D-DIC and a

hyperelastic anisotropic constitutive model. *Computer methods in biomechanics and biomedical engineering* **15**, 37–48.

BADIMON, L., PADRÓ, T. & VILAHUR, G. (2012). Atherosclerosis, platelets and thrombosis in acute ischaemic heart disease. *European heart journal. Acute cardiovascular care* **1**, 60–74.

BARTON, M., HAUDENSCHILD, C. C., D'USCIO, L. V, SHAW, S., MÜNTER, K. & LÜSCHER, T. F. (1998). Endothelin ETA receptor blockade restores NO-mediated endothelial function and inhibits atherosclerosis in apolipoprotein E-deficient mice. *Proceedings of the National Academy of Sciences of the United States of America* **95**, 14367–72.

BATES, D., MÄCHLER, M., BOLKER, B. & WALKER, S. (2014). Fitting Linear Mixed-Effects Models using lme4. 51.

BENNETT, H. S. (1950). *Methods applicable to the study of both fresh and fixed materials: the microscopical investigation of biological materials with polarized light*. McClug, J. R. (Ed.). New York: PB Hoeber Inc.

BENVENUTI, L. A., ONISHI, R. Y., GUTIERREZ, P. S. & HIGUCHI, M. DE L. (2005). Different patterns of atherosclerotic remodeling in the thoracic and abdominal aorta. *Clinics* **60**, 355–360.

BODE, M. K., MOSORIN, M., SATTA, J., RISTELI, L., JUVONEN, T. & RISTELI, J. (1999). Complete Processing of Type III Collagen in Atherosclerotic Plaques. *Arteriosclerosis, Thrombosis, and Vascular Biology* **19**, 1506–1511.

BONTHU, S., HEISTAD, D. D., CHAPPELL, D. A., LAMPING, K. G. & FARACI, F. M. (1997). Atherosclerosis, vascular remodeling, and impairment of

96

endothelium-dependent relaxation in genetically altered hyperlipidemic mice. *Arteriosclerosis, thrombosis, and vascular biology* **17**, 2333–40.

BOOT-HANDFORD, R. P., TUCKWELL, D. S., PLUMB, D. A., ROCK, C. F. & POULSOM, R. (2003). A novel and highly conserved collagen (pro(alpha)1(XXVII)) with a unique expression pattern and unusual molecular characteristics establishes a new clade within the vertebrate fibrillar collagen family. *The Journal of biological chemistry* **278**, 31067–77.

BROWN, E., MCKEE, T., DITOMASO, E., PLUEN, A., SEED, B., BOUCHER, Y. & JAIN, R. K. (2003). Dynamic imaging of collagen and its modulation in tumors in vivo using second-harmonic generation. *Nature medicine* **9**, 796–800.

BUCK, R. C. The fine structure of the aortic endothelial lesions in experimental cholesterol atherosclerosis of rabbits. *The American journal of pathology* **34**, 897–909.

CAMPAGNOLA, P. J., MILLARD, A. C., TERASAKI, M., HOPPE, P. E., MALONE, C. J. & MOHLER, W. A. (2002). Three-dimensional high-resolution second-harmonic generation imaging of endogenous structural proteins in biological tissues. *Biophysical journal* **82**, 493–508.

CANHAM, P. B., FINLAY, H. M. & TONG, S. Y. (1996). Stereological analysis of the layered collagen of human intracranial aneurysms. *Journal of microscopy* **183**, 170–80.

CARO, C. G., FITZ-GERALD, J. M. & SCHROTER, R. C. (1971). Atheroma and Arterial Wall Shear Observation, Correlation and Proposal of a Shear Dependent Mass Transfer Mechanism for Atherogenesis. *Proceedings of the Royal*

97

*Society B: Biological Sciences* **177**, 109–133.

CHEN, S.-Y., HSU, C.-Y. S. & SUN, C.-K. (2008). Epi-third and second harmonic generation microscopic imaging of abnormal enamel. *Optics Express* **16**, 11670–11679.

CHEN, W.-L., LI, T.-H., SU, P.-J., CHOU, C.-K., FWU, P. T., LIN, S.-J., KIM, D., SO, P. T. C. & DONG, C.-Y. (2010). <title>Second-order susceptibility imaging with polarization-resolved second harmonic generation microscopy</title>. In *BiOS*, Periasamy, A., So, P. T. C. & König, K. (Eds.), p. 75691P–75691P–7.

CHU, S.-W., CHEN, S.-Y., CHERN, G.-W., TSAI, T.-H., CHEN, Y.-C., LIN, B.-L. & SUN, C.-K. (2004). Studies of chi(2)/chi(3) tensors in submicron-scaled bio-tissues by polarization harmonics optical microscopy. *Biophysical journal* **86**, 3914–22.

CHU, S.-W., TAI, S.-P., CHAN, M.-C., SUN, C.-K., HSIAO, I.-C., LIN, C.-H., CHEN, Y.-C. & LIN, B.-L. (2007). Thickness dependence of optical second harmonic generation in collagen fibrils. *Optics Express* **15**, 12005.

CLARK, J. M. & GLAGOV, S. (1979). Structural integration of the arterial wall. I. Relationships and attachments of medial smooth muscle cells in normally distended and hyperdistended aortas. *Laboratory investigation; a journal of technical methods and pathology* **40**, 587–602.

COLLINS, M. J., BERSI, M., WILSON, E. & HUMPHREY, J. D. (2011). Mechanical properties of suprarenal and infrarenal abdominal aorta: implications for mouse models of aneurysms. *Medical engineering & physics* **33**, 1262–9.

COX, G. & KABLE, E. (2006). Second-harmonic imaging of collagen. *Methods in*

*molecular biology (Clifton, N.J.)* **319**, 15–35.

COX, G., KABLE, E., JONES, A., FRASER, I., MANCONI, F. & GORRELL, M. D. (2003). 3-Dimensional imaging of collagen using second harmonic generation. *Journal of Structural Biology* **141**, 53–62.

CRAUWELS, H. M., VAN HOVE, C. E., HOLVOET, P., HERMAN, A. G. & BULT, H. (2003). Plaque-associated endothelial dysfunction in apolipoprotein E-deficient mice on a regular diet. Effect of human apolipoprotein AI. *Cardiovascular research* **59**, 189–99.

DAVIES, M. J., RICHARDSON, P. D., WOOLF, N., KATZ, D. R. & MANN, J. (1993). Risk of thrombosis in human atherosclerotic plaques: role of extracellular lipid, macrophage, and smooth muscle cell content. *Heart* **69**, 377–381.

DECKERT, V., LIZARD, G., DUVERGER, N., ATHIAS, A., PALLEAU, V., EMMANUEL, F., MOISANT, M., GAMBERT, P., LALLEMANT, C. & LAGROST, L. (1999). Impairment of endothelium-dependent arterial relaxation by high-fat feeding in ApoE-deficient mice: toward normalization by human ApoA-I expression. *Circulation* **100**, 1230–5.

DENK, W., STRICKLER, J. H. & WEBB, W. W. (1990). Two-photon laser scanning fluorescence microscopy. *Science (New York, N.Y.)* **248**, 73–6.

DORAS, C., TAUPIER, G., BARSELLA, A., MAGER, L., BOEGLIN, A., BULOU, H., BOUSQUET, P. & DORKENOO, K. D. (2011a). Polarization state studies in second harmonic generation signals to trace atherosclerosis lesions. *Optics express* **19**, 15062–8.

——— (2011b). Polarization state studies in second harmonic generation

signals to trace atherosclerosis lesions. *Optics express* **19**, 15062–8.

DRIESSEN, N. J. B., COX, M. A. J., BOUTEN, C. V. C. & BAAIJENS, F. P. T. (2008). Remodelling of the angular collagen fiber distribution in cardiovascular tissues. *Biomechanics and modeling in mechanobiology* **7**, 93–103.

DURAN-STRUUCK, R. & DYSKO, R. C. (2009). Principles of bone marrow transplantation (BMT): providing optimal veterinary and husbandry care to irradiated mice in BMT studies. *Journal of the American Association for Laboratory Animal Science : JAALAS* **48**, 11–22.

D'USCIO, L. V, BARTON, M., SHAW, S. & LÜSCHER, T. F. (2002). Chronic ET(A) receptor blockade prevents endothelial dysfunction of small arteries in apolipoprotein E-deficient mice. *Cardiovascular research* **53**, 487–95.

EBERTH, J. F., GRESHAM, V. C., REDDY, A. K., POPOVIC, N., WILSON, E. & HUMPHREY, J. D. (2009). Importance of pulsatility in hypertensive carotid artery growth and remodeling. *Journal of hypertension* **27**, 2010–21.

ERIKSON, A., ORTEGREN, J., HOMPLAND, T., DE LANGE DAVIES, C. & LINDGREN, M. Quantification of the second-order nonlinear susceptibility of collagen I using a laser scanning microscope. *Journal of biomedical optics* **12**, 044002.

EXPOSITO, J.-Y., CLUZEL, C., GARRONE, R. & LETHIAS, C. (2002). Evolution of collagens. *The Anatomical record* **268**, 302–16.

FETTERMAN, J. L., POMPILIUS, M., WESTBROOK, D. G., UYEMINAMI, D., BROWN, J., PINKERTON, K. E. & BALLINGER, S. W. (2013). Developmental exposure to second-hand smoke increases adult atherogenesis and alters mitochondrial DNA copy number and deletions in apoE(-/-) mice. *PloS one* **8**, e66835.

FINLAY, H. M., MCCULLOUGH, L. & CANHAM, P. B. Three-dimensional collagen organization of human brain arteries at different transmural pressures. *Journal of vascular research* **32**, 301–12.

FRANKEN, P., HILL, A., PETERS, C. & WEINREICH, G. (1961). Generation of Optical Harmonics. *Physical Review Letters* **7**, 118–119.

FROSTEGÅRD, J. (2013). Immunity, atherosclerosis and cardiovascular disease. *BMC medicine* **11**, 117.

GALIS, Z. S. & KHATRI, J. J. (2002). Matrix Metalloproteinases in Vascular Remodeling and Atherogenesis: The Good, the Bad, and the Ugly. *Circ.*

GANNAWAY, J. N. & SHEPPARD, C. J. R. (1978). Second-harmonic imaging in the scanning optical microscope. *Optical and Quantum Electronics* **10**, 435–439.

GASSER, T. C., OGDEN, R. W. & HOLZAPFEL, G. A. (2006). Hyperelastic modelling of arterial layers with distributed collagen fibre orientations. *Journal of the Royal Society, Interface / the Royal Society* **3**, 15–35.

GAUDERON, R., LUKINS, P. B. & SHEPPARD, C. J. (2001). Simultaneous multichannel nonlinear imaging: combined two-photon excited fluorescence and second-harmonic generation microscopy. *Micron (Oxford, England : 1993)* **32**, 685–9.

GEORGE, M. H., MORGAN, J. B., GLOCK, R. D., TATUM, J. D., SCHMIDT, G. R., SOFOS, J. N., COWMAN, G. L. & SMITH, G. C. (1995). Injection-site lesions: incidence, tissue histology, collagen concentration, and muscle tenderness in beef rounds. *Journal of animal science* **73**, 3510–8.

GEORGIOU, E., THEODOSSIOU, T., HOVHANNISYAN, V., POLITOPOULOS, K., RAPTI, G. .

& YOVA, D. (2000). Second and third optical harmonic generation in type I collagen, by nanosecond laser irradiation, over a broad spectral region. *Optics Communications* **176**, 253–260.

GERVAIS, M., PONS, S., NICOLETTI, A., COSSON, C., GIUDICELLI, J.-F. & RICHER, C. (2003). Fluvastatin prevents renal dysfunction and vascular NO deficit in apolipoprotein E-deficient mice. *Arteriosclerosis, thrombosis, and vascular biology* **23**, 183–9.

GUO, X. & KASSAB, G. S. (2003). Variation of mechanical properties along the length of the aorta in C57bl/6 mice. *American journal of physiology. Heart and circulatory physiology* **285**, H2614–22.

GUNS, P.-J., VAN ASSCHE, T., VERRETH, W., FRANSEN, P., MACKNESS, B., MACKNESS, M., HOLVOET, P. & BULT, H. (2008). Paraoxonase 1 gene transfer lowers vascular oxidative stress and improves vasomotor function in apolipoprotein E-deficient mice with pre-existing atherosclerosis. *British journal of pharmacology* **153**, 508–16.

HADI, H. A. R., CARR, C. S. & AL SUWAIDI, J. (2005). Endothelial dysfunction: cardiovascular risk factors, therapy, and outcome. *Vascular health and risk management* **1**, 183–98.

HAMAMDZIC, D. & WILENSKY, R. L. (2013). Porcine models of accelerated coronary atherosclerosis: role of diabetes mellitus and hypercholesterolemia. *Journal of diabetes research* **2013**, 761415.

HELLENTHAL, F. A. M. V. I., GEENEN, I. L. A., TEIJINK, J. A. W., HEENEMAN, S. & SCHURINK, G. W. H. (2009). Histological features of human abdominal aortic

102

aneurysm are not related to clinical characteristics. *Cardiovascular pathology : the official journal of the Society for Cardiovascular Pathology* **18**, 286–93.

HILL, M. R., DUAN, X., GIBSON, G. A., WATKINS, S. & ROBERTSON, A. M. (2012). A theoretical and non-destructive experimental approach for direct inclusion of measured collagen orientation and recruitment into mechanical models of the artery wall. *Journal of biomechanics* **45**, 762–71.

HOLZAPFEL, G. (2000). Biomechanics of Soft Tissues. In *Computational Mechanics*. www.cis.tu-graz.ac.at/biomech.

HOLZAPFEL, G. A. (2001). *Handbook of Materials Behavior Models*. Elsevier http://www.sciencedirect.com/science/article/pii/B9780124433410501071

HOLZAPFEL, G. A., GASSER, T. C. & STADLER, M. (2002). A structural model for the viscoelastic behavior of arterial walls: Continuum formulation and finite element analysis. *European Journal of Mechanics - A/Solids* **21**, 441–463.

HOLZAPFEL, G. A. & OGDEN, R. W. (2010). Modelling the layer-specific three-dimensional residual stresses in arteries, with an application to the human aorta. *Journal of the Royal Society, Interface / the Royal Society* **7**, 787–99.

HOLZAPFEL, G. A., NIESTRAWSKA, J. A., OGDEN, R. W., REINISCH, A. J. & SCHRIEFL, A. J. (2015). Modelling non-symmetric collagen fibre dispersion in arterial walls. *Journal of the Royal Society, Interface / the Royal Society* **12**, 20150188–.

HULMES, DJS. (2008). Collagen diversity, synthesis and assembly. *Pan Vascular Medicine*. Berlin, Heidelberg: Springer Berlin Heidelberg, 15-47.

103

ISSELBACHER, E. M. (2005). Thoracic and abdominal aortic aneurysms. *Circulation*
**111**, 816–28.

JAMKHANDE, P. G., CHANDAK, P. G., DHAWALE, S. C., BARDE, S. R., TIDKE, P. S. &
SAKHARE, R. S. (2014). Therapeutic approaches to drug targets in
atherosclerosis. *Saudi pharmaceutical journal : SPJ : the official publication
of the Saudi Pharmaceutical Society* **22**, 179–90.

JAWIEN, J., TOTON-ZURANSKA, J., GAJDA, M., NIEPSUJ, A., GEBSKA, A., KUS, K.,
SUSKI, M., PYKA-FOSCIAK, G., NOWAK, B., GUZIK, T. J., MARCINKIEWICZ, J.,
OLSZANECKI, R. & KORBUT, R. (2012). Angiotensin-(1-7) receptor Mas agonist
ameliorates progress of atherosclerosis in apoE-knockout mice. *Journal of
physiology and pharmacology : an official journal of the Polish Physiological
Society* **63**, 77–85.

JEMAL, A., SIEGEL, R., WARD, E., MURRAY, T., XU, J., SMIGAL, C. & THUN, M. J.
Cancer statistics, 2006. *CA: a cancer journal for clinicians* **56**, 106–30.

JIANG, F., GIBSON, A. P. & DUSTING, G. J. (2001). Endothelial dysfunction induced
by oxidized low-density lipoproteins in isolated mouse aorta: a comparison
with apolipoprotein-E deficient mice. *European journal of pharmacology* **424**,
141–9.

JOHANSSON, M. E., HÄGG, U., WIKSTRÖM, J., WICKMAN, A., BERGSTRÖM, G. & GAN,
L. (2005). Haemodynamically significant plaque formation and regional
endothelial dysfunction in cholesterol-fed ApoE-/- mice. *Clinical science
(London, England : 1979)* **108**, 531–8.

JUNQUEIRA, L. C., BIGNOLAS, G. & BRENTANI, R. R. (1979). Picrosirius staining plus

polarization microscopy, a specific method for collagen detection in tissue sections. *The Histochemical journal* **11**, 447–55.

KATSUDA, S., OKADA, Y., MINAMOTO, T., ODA, Y., MATSUI, Y. & NAKANISHI, I. (1992). Collagens in human atherosclerosis. Immunohistochemical analysis using collagen type-specific antibodies. *Arteriosclerosis, Thrombosis, and Vascular Biology* **12**, 494–502.

KIM, B. M., EICHLER, J., REISER, K. M., RUBENCHIK, A. M. & DA SILVA, L. B. (2000). Collagen structure and nonlinear susceptibility: effects of heat, glycation, and enzymatic cleavage on second harmonic signal intensity. *Lasers in surgery and medicine* **27**, 329–35.

KNOWLES, J. W. & MAEDA, N. (2000). Genetic modifiers of atherosclerosis in mice. *Arteriosclerosis, thrombosis, and vascular biology* **20**, 2336–45.

KOCH, M., LAUB, F., ZHOU, P., HAHN, R. A., TANAKA, S., BURGESON, R. E., GERECKE, D. R., RAMIREZ, F. & GORDON, M. K. (2003). Collagen XXIV, a vertebrate fibrillar collagen with structural features of invertebrate collagens: selective expression in developing cornea and bone. *The Journal of biological chemistry* **278**, 43236–44.

KOLODGIE, F. D., KATOCS, A. S., LARGIS, E. E., WRENN, S. M., CORNHILL, J. F., HERDERICK, E. E., LEE, S. J. & VIRMANI, R. (1996). Hypercholesterolemia in the Rabbit Induced by Feeding Graded Amounts of Low-Level Cholesterol: Methodological Considerations Regarding Individual Variability in Response to Dietary Cholesterol and Development of Lesion Type. *Arteriosclerosis, Thrombosis, and Vascular Biology* **16**, 1454–1464.

KOSS, L. G. (1992). *Diagnostic cytology and its histopathologic bases*. Lippincott.

KU, D. N., GIDDENS, D. P., ZARINS, C. K. & GLAGOV, S. (1985). Pulsatile flow and atherosclerosis in the human carotid bifurcation. Positive correlation between plaque location and low oscillating shear stress. *Arteriosclerosis, Thrombosis, and Vascular Biology* **5**, 293–302.

LE, T. T., LANGOHR, I. M., LOCKER, M. J., STUREK, M. & CHENG, J.-X. (2007). Label-free molecular imaging of atherosclerotic lesions using multimodal nonlinear optical microscopy. *Journal of biomedical optics* **12**, 054007.

LEVENE, C.I. & POOLE, J.C. (1962). The collagen content of the normal and atherosclerotic human aortic intima. *British journal of experimental pathology* **43**, 469–71.

LI, D. & ROBERTSON, A. M. (2009). A structural multi-mechanism damage model for cerebral arterial tissue. *Journal of biomechanical engineering* **131**, 101013.

LIBBY, P. (2002). Inflammation in atherosclerosis. *Nature* **420**, 868–74.

LIBBY, P. (2015). Triglycerides on the rise: should we swap seats on the seesaw? *European heart journal* **36**, 774–6.

LIBBY, P. (2003). Vascular biology of atherosclerosis: overview and state of the art. *The American Journal of Cardiology* **91**, 3–6.

LIBBY, P., RIDKER, P. M. & HANSSON, G. K. (2009). Inflammation in atherosclerosis: from pathophysiology to practice. *Journal of the American College of Cardiology* **54**, 2129–38.

LIM, R. S., KRATZER, A., BARRY, N. P., MIYAZAKI-ANZAI, S., MIYAZAKI, M., MANTULIN,

W. W., LEVI, M., POTMA, E. O. & TROMBERG, B. J. (2010). Multimodal CARS microscopy determination of the impact of diet on macrophage infiltration and lipid accumulation on plaque formation in ApoE-deficient mice. *The Journal of Lipid Research* **51**, 1729–1737.

LIU, H., QIN, W., SHAO, Y., MA, Z., YE, T., BORG, T. & GAO, B. Z. (2011a). Myofibrillogenesis in live neonatal cardiomyocytes observed with hybrid two-photon excitation fluorescence-second harmonic generation microscopy. *Journal of biomedical optics* **16**, 126012.

———— (2011b). Myofibrillogenesis in live neonatal cardiomyocytes observed with hybrid two-photon excitation fluorescence-second harmonic generation microscopy. *Journal of biomedical optics* **16**, 126012.

LIU, H., SHAO, Y., QIN, W., RUNYAN, R. B., XU, M., MA, Z., BORG, T. K., MARKWALD, R. & GAO, B. Z. (2013). Myosin filament assembly onto myofibrils in live neonatal cardiomyocytes observed by TPEF-SHG microscopy. *Cardiovascular research* **97**, 262–70.

LODISH, H., BERK, A., ZIPURSKY, S. L., MATSUDAIRA, P., BALTIMORE, D. & DARNELL, J. (2000). Collagen: The Fibrous Proteins of the Matrix.

LUTTUN, A., LUTGENS, E., MANDERVELD, A., MARIS, K., COLLEN, D., CARMELIET, P. & MOONS, L. (2004). Loss of matrix metalloproteinase-9 or matrix metalloproteinase-12 protects apolipoprotein E-deficient mice against atherosclerotic media destruction but differentially affects plaque growth. *Circulation* **109**, 1408–14.

MA, Y., WANG, W., ZHANG, J., LU, Y., WU, W., YAN, H. & WANG, Y. (2012).

Hyperlipidemia and atherosclerotic lesion development in Ldlr-deficient mice on a long-term high-fat diet. *PloS one* **7**, e35835.

MALEK, A. M. (1999). Hemodynamic Shear Stress and Its Role in Atherosclerosis. *JAMA* **282**, 2035.

MEIR, K. S. & LEITERSDORF, E. (2004). Atherosclerosis in the apolipoprotein-E-deficient mouse: a decade of progress. *Arteriosclerosis, thrombosis, and vascular biology* **24**, 1006–14.

MEYER, T., BAUMGARTL, M., GOTTSCHALL, T., PASCHER, T., WUTTIG, A., MATTHÄUS, C., ROMEIKE, B. F. M., BREHM, B. R., LIMPERT, J., TÜNNERMANN, A., GUNTINAS-LICHIUS, O., DIETZEK, B., SCHMITT, M. & POPP, J. (2013). A compact microscope setup for multimodal nonlinear imaging in clinics and its application to disease diagnostics. *The Analyst* **138**, 4048–57.

MORIN, C., HELLMICH, C., & AVRIL, S. (2015). The fiber reorientation problem revisited in the context of Eshelbian micromechanics: theory and computations. *Proc Appl Math Mech* **15**, 39-42.

MORISAKI, N., SAITO, I., TAMURA, K., TASHIRO, J., MASUDA, M., KANZAKI, T., WATANABE, S., MASUDA, Y. & SAITO, Y. (1997). New indices of ischemic heart disease and aging: studies on the serum levels of soluble intercellular adhesion molecule-1 (ICAM-1) and soluble vascular cell adhesion molecule-1 (VCAM-1) in patients with hypercholesterolemia and ischemic heart disease. *Atherosclerosis* **131**, 43–8.

MOSTAÇO-GUIDOLIN, L. B., KO, A. C.-T., WANG, F., XIANG, B., HEWKO, M., TIAN, G., MAJOR, A., SHIOMI, M. & SOWA, M. G. (2013). Collagen morphology and

texture analysis: from statistics to classification. *Scientific reports* **3**, 2190.

MOSTAÇO-GUIDOLIN, L. B., KO, A. C.-T., WANG, F., XIANG, B., HEWKO, M., TIAN, G., MAJOR, A., SHIOMI, M. & SOWA, M. G. (2013). Collagen morphology and texture analysis: from statistics to classification. *Scientific Reports* **3**, 2190.

MUELLER, M. M. & FUSENIG, N. E. (2002). Tumor-stroma interactions directing phenotype and progression of epithelial skin tumor cells. *Differentiation; research in biological diversity* **70**, 486–97.

MURPHY, E. & STEENBERGEN, C. (2007). Cardioprotection in females: a role for nitric oxide and altered gene expression. *Heart failure reviews* **12**, 293–300.

NAKASHIMA, Y., PLUMP, A. S., RAINES, E. W., BRESLOW, J. L. & ROSS, R. (1994). ApoE-deficient mice develop lesions of all phases of atherosclerosis throughout the arterial tree. *Arteriosclerosis, Thrombosis, and Vascular Biology* **14**, 133–140.

NAKASHIMA, Y., RAINES, E. W., PLUMP, A. S., BRESLOW, J. L. & ROSS, R. (1998). Upregulation of VCAM-1 and ICAM-1 at atherosclerosis-prone sites on the endothelium in the ApoE-deficient mouse. *Arteriosclerosis, thrombosis, and vascular biology* **18**, 842–51.

NAWAWI, H., OSMAN, N. S., ANNUAR, R., KHALID, B. A. K. & YUSOFF, K. (2003). Soluble intercellular adhesion molecule-1 and interleukin-6 levels reflect endothelial dysfunction in patients with primary hypercholesterolaemia treated with atorvastatin. *Atherosclerosis* **169**, 283–91.

NIH AND NHLBI (2012). *Chapter 4 Disease Statistics*. www.nhlbi.nih.gov/about/factbook/chapter4.htm#gr36.

NOGUEIRA, B. V, PEOTTA, V. A., MEYRELLES, S. S. & VASQUEZ, E. C. (2007). Evaluation of aortic remodeling in apolipoprotein E-deficient mice and renovascular hypertensive mice. *Archives of medical research* **38**, 816–21.

OSBORN, E. A. & JAFFER, F. A. (2013). Imaging atherosclerosis and risk of plaque rupture. *Current atherosclerosis reports* **15**, 359.

PACE, J. M., CORRADO, M., MISSERO, C. & BYERS, P. H. (2003). Identification, characterization and expression analysis of a new fibrillar collagen gene, COL27A1. *Matrix biology : journal of the International Society for Matrix Biology* **22**, 3–14.

PAGIDIPATI, N. J. & GAZIANO, T. A. (2013). Estimating deaths from cardiovascular disease: a review of global methodologies of mortality measurement.

PALERO, J. A., DE BRUIJN, H. S., VAN DER PLOEG VAN DEN HEUVEL, A., STERENBORG, H. J. C. M. & GERRITSEN, H. C. (2007). Spectrally resolved multiphoton imaging of in vivo and excised mouse skin tissues. *Biophysical journal* **93**, 992–1007.

PARK, K.-H. & PARK, W. J. (2015). Endothelial Dysfunction: Clinical Implications in Cardiovascular Disease and Therapeutic Approaches. *Journal of Korean medical science* **30**, 1213–25.

PEPINE, C. J. (1998). Clinical implications of endothelial dysfunction. *Clinical Cardiology* **21**, 795–799.

PHILLIP, J. M., AIFUWA, I., WALSTON, J. & WIRTZ, D. (2015). The Mechanobiology of Aging. *Annual review of biomedical engineering* **17**, 113–41.

PLOTNIKOV, S. V, MILLARD, A. C., CAMPAGNOLA, P. J. & MOHLER, W. A. (2006).

110

Characterization of the myosin-based source for second-harmonic generation from muscle sarcomeres. *Biophysical journal* **90**, 693–703.

PSILODIMITRAKOPOULOS, S., PETEGNIEF, V., DE VERA, N., HERNANDEZ, O., ARTIGAS, D., PLANAS, A. M. & LOZA-ALVAREZ, P. (2013). Quantitative imaging of microtubule alteration as an early marker of axonal degeneration after ischemia in neurons. *Biophysical journal* **104**, 968–75.

PUCHTLER, H., WALDROP, F. S. & VALENTINE, L. S. (1973). Polarization microscopic studies of connective tissue stained with picro-sirius red FBA. *Beiträge zur Pathologie* **150**, 174–87.

RAWLINS, J. M., LAM, W. L., KAROO, R. O., NAYLOR, I. L. & SHARPE, D. T. (2006). Quantifying Collagen Type in Mature Burn Scars: A Novel Approach Using Histology and Digital Image Analysis. *Journal of Burn Care & Research* **27**, 60–65.

RHODIN, J. (1980). *Architecture of the vessel wall*. 2nd ed. Sparks, G. S. (Ed.). Bethesda: American Physiological Society.

ROTH, S. & FREUND, I. (1981). Optical second-harmonic scattering in rat-tail tendon. *Biopolymers* **20**, 1271–90.

RUBBENS, M. P., DRIESSEN-MOL, A., BOERBOOM, R. A., KOPPERT, M. M. J., VAN ASSEN, H. C., TERHAAR ROMENY, B. M., BAAIJENS, F. P. T. & BOUTEN, C. V. C. (2009). Quantification of the temporal evolution of collagen orientation in mechanically conditioned engineered cardiovascular tissues. *Annals of biomedical engineering* **37**, 1263–72.

SÁNCHEZ, S. A., MÉNDEZ-BARBERO, N., SANTOS-BENEIT, A. M., ESTEBAN, V.,

JIMÉNEZ-BORREGUERO, L. J., CAMPANERO, M. R. & REDONDO, J. M. (2014). Nonlinear optical 3-dimensional method for quantifying atherosclerosis burden. *Circulation. Cardiovascular imaging* **7**, 566–9.

SCHENKE-LAYLAND, K., RIEMANN, I., STOCK, U. A. & KÖNIG, K. (2005). Imaging of cardiovascular structures using near-infrared femtosecond multiphoton laser scanning microscopy. *Journal of biomedical optics* **10**, 024017.

SCHRAUWEN, J. T. C., VILANOVA, A., REZAKHANIHA, R., STERGIOPULOS, N., VAN DE VOSSE, F. N. & BOVENDEERD, P. H. M. (2012). A method for the quantification of the pressure dependent 3D collagen configuration in the arterial adventitia. *Journal of structural biology* **180**, 335–42.

SCHRIEFL, A. J., REINISCH, A. J., SANKARAN, S., PIERCE, D. M. & HOLZAPFEL, G. A. (2012). Quantitative assessment of collagen fibre orientations from two-dimensional images of soft biological tissues. *Journal of the Royal Society, Interface / the Royal Society* **9**, 3081–93.

SCHRIEFL, A. J., ZEINDLINGER, G., PIERCE, D. M., REGITNIG, P. & HOLZAPFEL, G. A. (2011). Determination of the layer-specific distributed collagen fibre orientations in human thoracic and abdominal aortas and common iliac arteries. *Journal of The Royal Society Interface* **9**, 1275–1286.

STILL, W. J. S. & MARRIOTT, P. R. (1964). Comparative morphology of the early atherosclerotic lesion in man and cholesterol-atherosclerosis in the rabbit an electronmicroscopic study. *Journal of Atherosclerosis Research* **4**, 373–386.

STOLETOV, K., FANG, L., CHOI, S.-H., HARTVIGSEN, K., HANSEN, L. F., HALL, C., PATTISON, J., JULIANO, J., MILLER, E. R., ALMAZAN, F., CROSIER, P., WITZTUM,

J. L., KLEMKE, R. L. & MILLER, Y. I. (2009). Vascular lipid accumulation, lipoprotein oxidation, and macrophage lipid uptake in hypercholesterolemic zebrafish. *Circulation research* **104**, 952–60.

STOLLER, P., KIM, B.-M., RUBENCHIK, A. M., REISER, K. M. & DA SILVA, L. B. (2002). Polarization-dependent optical second-harmonic imaging of a rat-tail tendon. *Journal of biomedical optics* **7**, 205–14.

SU, J. B. (2015). Vascular endothelial dysfunction and pharmacological treatment. *World journal of cardiology* **7**, 719–41.

SUHALIM, J. L., CHUNG, C.-Y., LILLEDAHL, M. B., LIM, R. S., LEVI, M., TROMBERG, B. J. & POTMA, E. O. (2012). Characterization of Cholesterol Crystals in Atherosclerotic Plaques Using Stimulated Raman Scattering and Second-Harmonic Generation Microscopy. *Biophysical Journal* **102**, 1988–1995.

TANG, J., ZHANG, Y., ZHANG, M.-B., LI, Y.-M., FEI, X. & SONG, Z.-G. Tissue elasticity displayed by elastography and its correlation with the characteristics of collagen type I and type III in prostatic stroma. *Asian journal of andrology* **16**, 305–8.

TIAN, F., LI, J., LIU, X.-W., TONG, T.-J. & ZHANG, Z.-Y. (2015). Age-dependent accumulation of mitochondrial DNA deletions in the aortic root of atherosclerosis-prone apolipoprotein E-knockout mice. *Archives of gerontology and geriatrics* **63**, 72-77.

TSAMIS, A., KRAWIEC, J. T. & VORP, D. A. (2013). Elastin and collagen fibre microstructure of the human aorta in ageing and disease: a review. *Journal of the Royal Society, Interface / the Royal Society* **10**, 20121004.

113

TUNSTALL-PEDOE, H. (2006). Preventing Chronic Diseases. A Vital Investment: WHO Global Report. Geneva: World Health Organization, 2005. pp 200. CHF 30.00. ISBN 92 4 1563001. *International Journal of Epidemiology* **35**, 1107–1107.

VAN DER REST, M. & GARRONE, R. (1991). Collagen family of proteins. *FASEB journal : official publication of the Federation of American Societies for Experimental Biology* **5**, 2814–23.

VIRMANI, R., BURKE, A. P., FARB, A. & KOLODGIE, F. D. (2006). Pathology of the vulnerable plaque. *Journal of the American College of Cardiology* **47**, C13–8.

VON DER MARK, K. (1981). Localization of collagen types in tissues. *International review of connective tissue research* **9**, 265–324.

VUORIO, E. & DE CROMBRUGGHE, B. (1990). The family of collagen genes. *Annual review of biochemistry* **59**, 837–72.

WANG, H.-W., LANGOHR, I. M., STUREK, M. & CHENG, J.-X. (2009). Imaging and Quantitative Analysis of Atherosclerotic Lesions by CARS-Based Multimodal Nonlinear Optical Microscopy. *Arteriosclerosis, Thrombosis, and Vascular Biology* **29**, 1342–1348.

WANG, J. C. & BENNETT, M. (2012). Aging and Atherosclerosis: Mechanisms, Functional Consequences, and Potential Therapeutics for Cellular Senescence. *Circulation Research* **111**, 245–259.

WARD, N. P., HULMES, D. J. S. & CHAPMAN, J. A. (1986). Collagen self-assembly in vitro: Electron microscopy of initial aggregates formed during the lag phase.

*Journal of Molecular Biology* **190**, 107–112.

WASSMANN, S., WERNER, N., CZECH, T. & NICKENIG, G. (2006). Improvement of endothelial function by systemic transfusion of vascular progenitor cells. *Circulation research* **99**, e74–83.

WATSON, S., LIU, P., PENA, E., SUTTON, M., EBERTH, J. & LESSNER, S. (2015). Diet-induced Vascular Remodeling Produces a Shift in Collagen Fiber Angle Distribution in a Mouse Model of Atherosclerosis. *FASEB J* **29**, 719.9–.

WATSON, S. R., LIU, P., PEÑA, E. A., SUTTON, M. A., EBERTH, J. F. & LESSNER, S. M. (2016). Comparison of Aortic Collagen Fiber Angle Distribution in Mouse Models of Atherosclerosis Using Second-Harmonic Generation (SHG) Microscopy. *Microscopy and microanalysis :*volume 1-8.

WEINGÄRTNER, O., HUSCHE, C., SCHÖTT, H. F., SPEER, T., BÖHM, M., MILLER, C. M., MCCARTHY, F., PLAT, J., LÜTJOHANN, D. & LAUFS, U. (2015). Vascular effects of oxysterols and oxyphytosterols in apoE -/- mice. *Atherosclerosis* **240**, 73–9.

WHITMAN, S. C. (2004). A practical approach to using mice in atherosclerosis research. *The Clinical biochemist. Reviews / Australian Association of Clinical Biochemists* **25**, 81–93.

WICKER, B. K., HUTCHENS, H. P., WU, Q., YEH, A. T. & HUMPHREY, J. D. (2008). Normal basilar artery structure and biaxial mechanical behaviour.

WILLIAMS, R. M., ZIPFEL, W. R. & WEBB, W. W. (2005). Interpreting second-harmonic generation images of collagen I fibrils. *Biophysical journal* **88**, 1377–86.

115

WOLINSKY, H. & GLAGOV, S. (1969). Comparison of Abdominal and Thoracic Aortic Medial Structure in Mammals. *Circulation Research* **25**, 677–686.

YI, X., XU, L., KIM, K., KIM, H.-S. & MAEDA, N. (2010). Genetic reduction of lipoic acid synthase expression modestly increases atherosclerosis in male, but not in female, apolipoprotein E-deficient mice. *Atherosclerosis* **211**, 424–30.

YONESHIGE, A., HAGIYAMA, M., FUJITA, M. & ITO, A. (2015). Pathogenic Actions of Cell Adhesion Molecule 1 in Pulmonary Emphysema and Atopic Dermatitis. *Frontiers in cell and developmental biology* **3**, 75.

YU, W., BRAZ, J. C., DUTTON, A. M., PRUSAKOV, P. & REKHTER, M. In vivo imaging of atherosclerotic plaques in apolipoprotein E deficient mice using nonlinear microscopy. *Journal of biomedical optics* **12**, 054008.

ZHANG, S. H., REDDICK, R. L., PIEDRAHITA, J. A. & MAEDA, N. (1992). Spontaneous hypercholesterolemia and arterial lesions in mice lacking apolipoprotein E. *Science (New York, N.Y.)* **258**, 468–71.

ZIPFEL, W. R., WILLIAMS, R. M., CHRISTIE, R., NIKITIN, A. Y., HYMAN, B. T. & WEBB, W. W. (2003). Live tissue intrinsic emission microscopy using multiphoton-excited native fluorescence and second harmonic generation. *Proceedings of the National Academy of Sciences of the United States of America* **100**, 7075–80.

ZOUMI, A., LU, X., KASSAB, G. S. & TROMBERG, B. J. (2004). Imaging coronary artery microstructure using second-harmonic and two-photon fluorescence microscopy. *Biophysical journal* **87**, 2778–86.

# APPENDIX A: COPYRIGHT PERMISSION

**To:** Shana Watson;

● You forwarded this message on 4/6/2016 3:14 PM.

| Bing Maps | | + Get more apps |
| --- | --- | --- |

Dear Ms. Watson,

Permission is not required for authors who wish to re-use material they have written for a Cambridge publication, provided the subsequent use includes a full acknowledgement of the original publication, together with the copyright notice and the phrase 'Reprinted with permission'. For a fuller description of this policy, please view the policy on our website: http://www.cambridge.org/us/about-us/rights-permissions/permissions/permissions-requests-our-authors/.

Regards,


Adam Hirschberg
Senior Permissions Associate
Cambridge University Press
32 Avenue of the Americas
New York, NY 10013-2473

tel.: 212-337-5088 (direct)
tel.: 212-924-3900 (general)
fax: 212-691-3239 (general)
email: ahirschberg@cambridge.org
web: www.cambridge.org/us


Figure A.1: Above is proof that Chapter 2 and Chapter 3 include full-text that was reprinted with permission from a Cambridge Journal, *Microscopy and Microanalysis.*

117